AD-A050 037 SRI INTERNATIONAL MENLO PARK CA MOLECULAR PHYSICS CENTER F/G 20/8
INELASTIC COLLISIONS OF EXCITED ATOMS.(U)
JAN 78 K T GILLEN N00014-76-C-0118
UNCLASSIFIED SRI-MP-78-13 NL

1 OF 1
AD A050 037

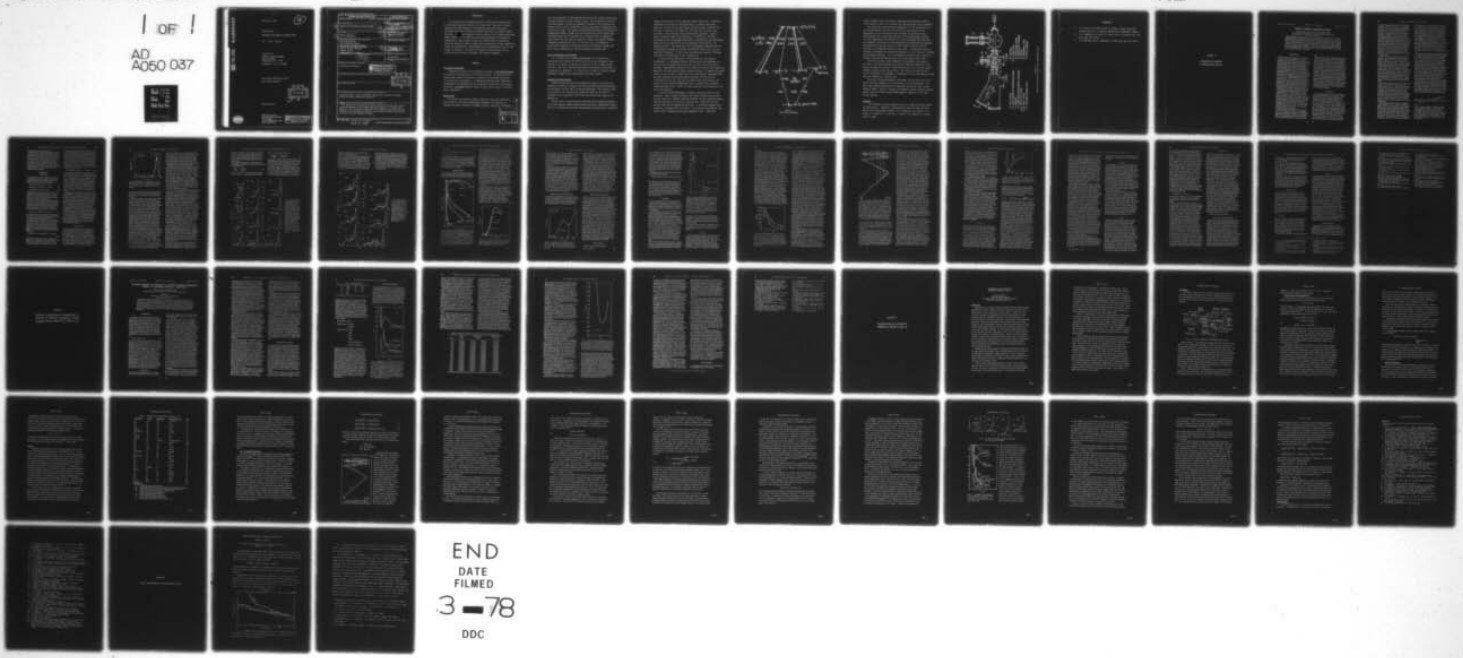

END
DATE FILMED
3-78
DDC

January 31, 1978

12
B.S.

Annual Report

INELASTIC COLLISIONS OF EXCITED ATOMS

By: Keith T. Gillen

Prepared for

OFFICE OF NAVAL RESEARCH
Physics Branch
Washington, D.C. 20360

Attention: Dr. B. R. Junker

ONR Contract N00014-76-C-0118

SRI Project PYU-4529

Report MP 78-13

SRI International

333 Ravenswood Ave.
Menlo Park, California 94025
(415) 326-6200
Cable: STANRES, Menlo Park
TWX: 910-373-1246

SECURITY CLASSIFICATION OF THIS PAGE *(When Data Entered)*

REPORT DOCUMENTATION PAGE

READ INSTRUCTIONS BEFORE COMPLETING FORM

1. REPORT NUMBER

2. GOVT ACCESSION NO.

3. RECIPIENT'S CATALOG NUMBER

4. TITLE *(and Subtitle)*

INELASTIC COLLISIONS OF EXCITED ATOMS.

5. TYPE OF REPORT & PERIOD COVERED

Annual Report.
October 1976-December 1977

6. PERFORMING ORG. REPORT NUMBER

SRI - MP-78-13

7. AUTHOR(s)

Keith T. Gillen

8. CONTRACT OR GRANT NUMBER(s)

N000014-76-C-0118

9. PERFORMING ORGANIZATION NAME AND ADDRESS

SRI International
333 Ravenswood Avenue
Menlo Park, California 94025

10. PROGRAM ELEMENT, PROJECT, TASK AREA & WORK UNIT NUMBERS

11. CONTROLLING OFFICE NAME AND ADDRESS

Office of Naval Research
Physics Branch
Washington, D.C. 20360

12. REPORT DATE

31 January 1978

13. NUMBER OF PAGES

56

14. MONITORING AGENCY NAME & ADDRESS *(if different from Controlling Office)*

58p.

15. SECURITY CLASS. *(of this report)*

Unclassified

15a. DECLASSIFICATION/DOWNGRADING SCHEDULE

16. DISTRIBUTION STATEMENT *(of this Report)*

Distribution unlimited.

DISTRIBUTION STATEMENT A
Approved for public release;
Distribution Unlimited

17. DISTRIBUTION STATEMENT *(of the abstract entered in Block 20, if different from Report)*

DDC
RECEIVED
FEB 15 1978
B

18. SUPPLEMENTARY NOTES

19. KEY WORDS *(Continue on reverse side if necessary and identify by block number)*

metastable atoms; atomic collisions; ionization; excitation transfer; charge transfer; collisional excitation

20. ABSTRACT *(Continue on reverse side if necessary and identify by block number)*

The interaction of metastable rare gas atoms with ground state atoms is being investigated in the energy range from several eV to several keV. Emphasis is on collisional ionization and collisional excitation transfer. Additional work examines the details of the charge transfer reaction used to produce the fast metastable beams.

DD FORM 1 JAN 73 1473 EDITION OF 1 NOV 65 IS OBSOLETE

410 514

SB

SECURITY CLASSIFICATION OF THIS PAGE *(When Data Entered)*

INTRODUCTION

Our laboratory has pioneered research on collisions of excited atoms in the energy range from several eV to several keV. This work is aimed at improving the understanding of the fundamental mechanisms underlying electronic excitation transfer, collisional ionization, and charge transfer reactions. In work supported by this contract, we are studying relatively simple systems that are amenable to detailed experimental and theoretical investigation. Some of these systems have direct practical application; others are studied in order to predict the characteristics of more complicated systems by extrapolation. Understanding of these mechanisms is basic to any attempt to describe or anticipate the behavior of excited media such as visible and uv gas lasers, discharges, and excited atmospheres.

PROGRESS

Collisional Ionization

During the past year we have published two papers in The Physical Review on ionization of metastable He in collisions with He. The detailed experimental paper entitled "Ionization in Collisions of Metastable He with He" is included here as Appendix A. A companion theoretical paper "Theoretical Investigation of a Mechanism for Ion Production in Collisions of Metastable He with He: Ab initio Potential Curves for $^1\Sigma_g^+$ States of He_2" is included here as Appendix B.

Review Paper

Dr. Gillen was invited to present a lecture on the work supported by this contract at the Tenth International Conference on the Physics of Electron and Atomic Collisions (X ICPEAC) in Paris, July 1977. His address

was titled "Inelastic He Metastable-He Scattering" and reviewed recent work, here and elsewhere, on this collision system. For publication in the book of invited papers, the talk was expanded to include a short review of the present status of work on metastable rare gas collisions at energies in the electron volt range. This paper, entitled "Metastable Rare Gas Collisions of Intermediate Energies (5-3000 eV)," was written with partial support from this ONR contract and is included here, in preprint form, as Appendix C. Travel funds from this contract allowed Dr. Gillen to attend the X ICPEAC conference and present his talk. On the same trip, he attended the International Symposium on Ion-Atom Collisions in Darmstadt, Germany, and gave a short presentation on the SRI collisional ionization work.

Total Destruction Cross Sections

Dr. T. M. Miller has completed measurements of low energy total destruction cross sections for $He^*(2^3S)$ with He and has published a short summary of the results in the Book of Abstracts for the X ICPEAC, Paris, July 1977. The paper, "$He(2^3S)$ Deexcitation in Collisions with $He(1^1S)$" is included here as Appendix D. Dr. Miller was also able to attend the ICPEAC conference through partial travel support from this contract.

Completion of New Facility

During the past year we have broadened the scope of our program considerably by starting to address one of the most vexing problems associated with metastable rare gas (Rg^*) scattering experiments. This problem, which is not unique to our laboratory or production method, is the lack of knowledge of the composition of Rg^* beams (see discussion on pages 4-5 of Appendix C).

We plan first to characterize the metastable beam composition produced in the near-resonant charge transfer process and then to modify beam compositions for isolating the scattering contributions associated with a particular

component of the beam. We are using the tunable output from a stabilized single-mode cw dye laser to selectively excite a specific metastable component. For Ne, Ar, Kr, and Xe there are many allowed transitions for the outer s electron in the lowest $^3P_2$, $^3P_1$, $^3P_0$, and $^1P_1$ states [core $(n-1)p^5ns$] to the 10 nearest excited states [core $(n-1)p^5np$]. Figure 1 shows a convenient upper state ($2p^5 3p'[\frac{1}{2}]_1$) for $Ne^*(^3P_0)$ or $Ne^*(^3P_2)$ excitation and the wavelengths and Einstein A coefficients of the transitions between this level and the $^3P_2$ and $^3P_0$ metastable states and $^3P_1$, $^1P_1$ radiating states.[1] This upper state can be populated by pumping either the $^3P_2$ metastable component of the beam with 5881.9 Å light or the $^3P_0$ state with 6163.6 Å photons.[2] In both cases, the spontaneous emission branching ratios will be proportional to the A coefficients.

By using low excitation powers and monitoring the laser-induced fluorescence at a wavelength different from the excitation wavelength, we will be able to determine the ratio of the $^3P_0$ state to the $^3P_2$ state in the beam. Supplementary information[3] will yield the complete beam composition produced in the near-resonant charge transfer reaction. At higher laser power levels, we will be able to remove one of the two metastable components from the beam, determine the relative surface secondary electron ejection coefficients for the $^3P_2$, $^3P_0$, and $^1S_0$ (ground state) fast neutrals, and initiate various scattering experiments with a purified beam containing a single metastable state. Several of these experiments were described in our most recent proposal.

To initiate these experiments, we needed a substantial amount of new equipment: lasers, optical components, and signal processing electronics. The key items were a Coherent Radiation CR-599-21 actively stabilized single-mode dye laser and a Kr ion laser to pump the dye. Funds from this ONR contract were used to purchase the dye laser. A recent NSF equipment grant allowed us to purchase the Kr ion laser, a 0.5-m grating monochromator, and various optical components and optical diagnostic tools. Using SRI's

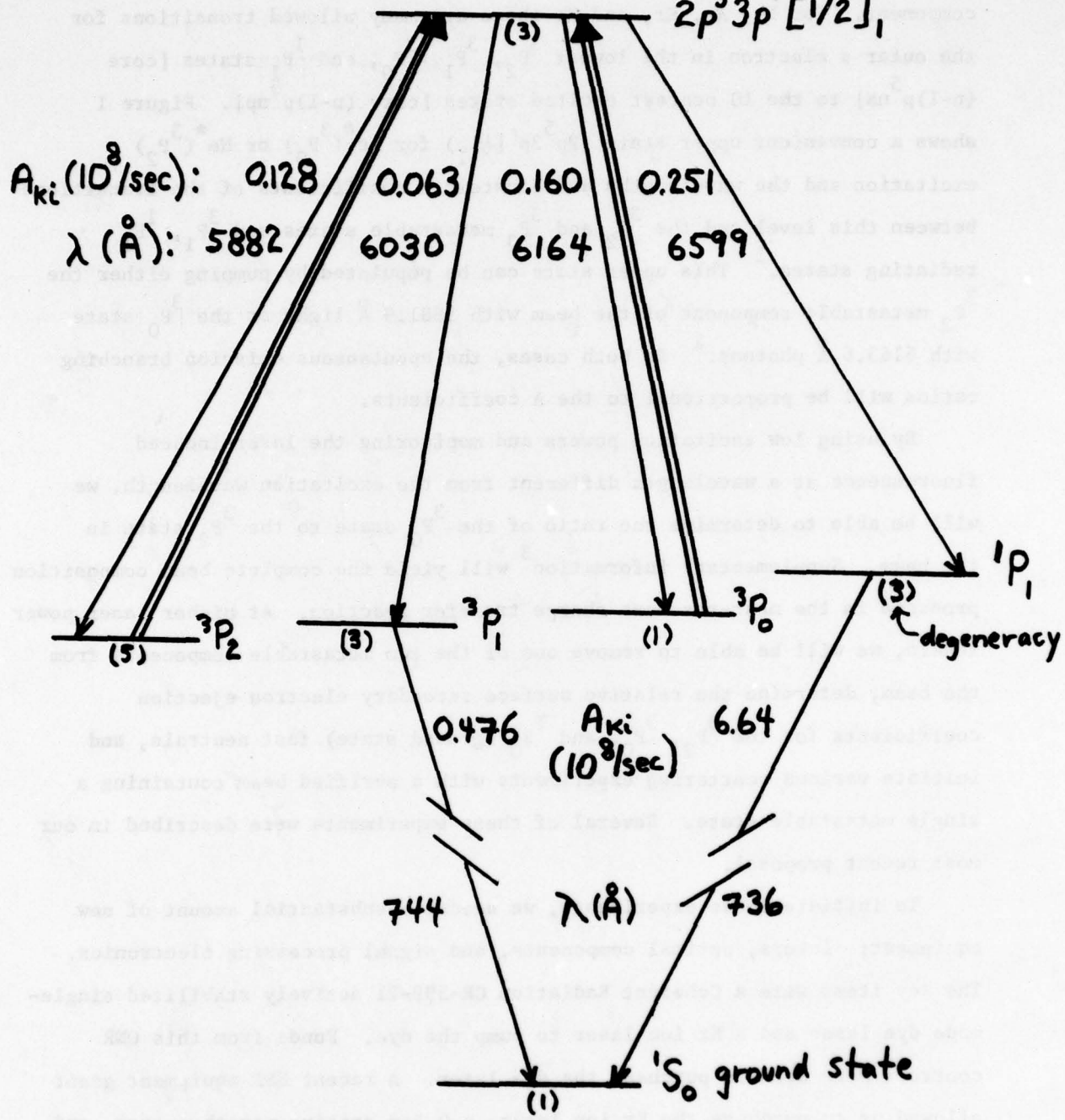

Figure 1
Neon Optical Pumping

capital equipment fund, we obtained a 4096-channel multichannel analyzer, a dual channel scaler, an X-Y plotter, and some additional optical equipment.

The metastable beam-purification experiments will be accomplished on an existing apparatus that was used in the past (see Appendix D) for measurements of total destruction cross sections for metastable beams. Unfortunately, the original apparatus was not in an environment suitable for laser experiments, and modification of the surrounding room would have been difficult, disruptive of other experiments, and prohibitively expensive. The apparatus has now been moved to a more suitable laboratory with an existing 5 x 12 honeycomb-reinforced laser table. A significant effort was required to reassemble and support the apparatus so as to isolate it reasonably from building vibrations. It is now supported on concrete piers physically separated from the building structure, as is the adjacent laser table.

The three principal vacuum chambers in the apparatus (see Figure 2), the source, the charge exchange oven, and the interaction region were each mounted on separate platforms. These units now rest on an all-steel welded framework mounted on the concrete piers. This structure allows for easy access, replacement, rearrangement, or modification of the experimental system, since each chamber is a separate unit.

The entire scattering apparatus, including a new ion source and a new photon detection assembly, is now operational in its new laboratory. The first laser pumping experiments will begin when the new dye laser arrives (February 1978). The move, redesign, and component testing received financial support from SRI internal funds and NSF funds, in addition to the support of this contract.

Personnel

J. R. Peterson is project supervisor and K. T. Gillen is project leader for this contract. Significant contributions to this work have also been made by the following SRI personnel: M. J. Coggiola, G. M. Conklin, T. D. Gaily, D. L. Huestis, R. L. Leon, D. C. Lorents, T. M. Miller, R. E. Olson and R. P. Saxon.

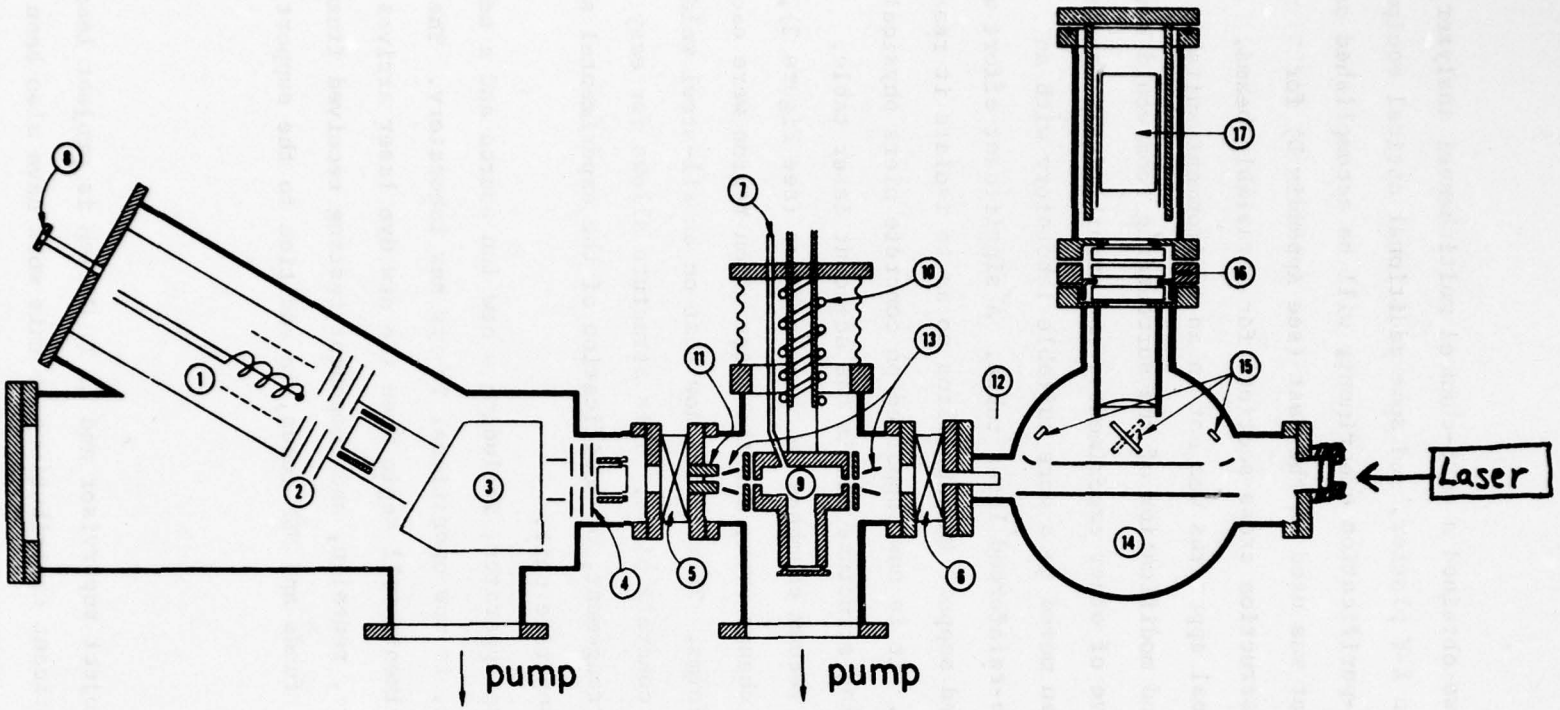

① Ion source
② Lens system & deflecting plates
③ Magnet
④ Lens system(retarding focussing)
⑤, ⑥ Shut-off valves
⑦, ⑧ Gas inlets
⑨ Charge transfer oven
⑩ Cooling
⑪, ⑫ Apertures
⑬ Deflecting plates
⑭ Observation Chamber
⑮ Mirrors
⑯ Interference filter
⑰ Photo multiplier

Figure 2

Facility for scattering pure state metastable beams

REFERENCES

1. W. L. Wiese, M. W. Smith, and B. M. Glennon, "Atomic Transition Probabilities, Vol. I, Hydrogen Through Neon," NSRDS:NBS 4 (1966).
2. F. B. Dunning, T. B. Cook, W. P. West, and R. F. Stebbings, Rev. Sci. Instr. 46, 1072 (1975).
3. R. H. Neynaber and G. D. Magnuson, J. Chem. Phys. 65, 5239 (1977).

Appendix A

IONIZATION IN COLLISIONS OF METASTABLE He WITH He

PHYSICAL REVIEW A VOLUME 15, NUMBER 2 FEBRUARY 1977

Ionization in collisions of metastable He with He†

Keith T. Gillen, James R. Peterson, and Ronald E. Olson
Molecular Physics Center, Stanford Research Institute, Menlo Park, California 94025
(Received 13 September 1976)

Detailed differential cross-section measurements have been performed for production of He^+ in collisions of metastable $He^*(2^3S$ and $2^1S)$ with He at center-of-mass energies of 50, 99, and 199 eV. The product ion distribution contains several distinct features dominated by an intense peak at small angles and an energy-loss value near threshold. The major features of the ionization are shown to be consistent with various calculated processes, each of which follows the Σ_g^+ diabatic repulsive potential on the incoming trajectory. Ionization occurs at the crossing into the continuum, at the classical inner turning point, at crossings with higher continua, and through molecular autoionization of doubly excited neutral states. Possible contributions from $He^+ + He^-$ autoionizing states are considered. Evidence is found for significant contributions to the ionization from the small amount of $He^*(2^1S)$ in the beam.

INTRODUCTION

The He_2 system is an ideal choice for the study of collisional processes because it is simple enough that accurate theoretical calculations can be compared with most experimental results. The interaction potentials can be obtained using *ab initio* techniques and the dynamical properties can be deduced from trajectory calculations on the relevant potential curves using estimates of the couplings between curves near crossings or avoided crossings. One of the important problems remaining to be understood in collision physics is the nature of the coupling between a discrete state and a continuum. Little detailed data exist for comparison with theory. Collisional ionization experiments in simple systems should contribute significantly to the understanding of the general problem, since the discrete state interactions are well enough understood that effort can be concentrated on the continuum coupling mechanisms.

In this paper we present a detailed study of collisional ionization in the scattering of a beam of metastable helium by helium target gas in the center-of-mass (c.m.) energy range 50–199 eV. Several ionization channels are identified by demonstrating that the deflection functions and energy losses calculated on the pertinent potential curves are consistent with the experimental results. A companion paper describes the calculation of the potential energy curves for the $^1\Sigma_g^+$ states of He_2, and demonstrates their relevance to one of the prominent ionization channels.

This experiment represents the first measurement of the collisional ionization of metastable He at low energies and contains the first detailed analysis of the product ion angle-energy distribution. In a preliminary publication we described the most intense feature of the collisional ionization.[1]

Several recent studies of ground-state rare-gas collisions in the energy range from several hundred to several thousand eV have examined the details of various ionization processes either by measurements of the emitted electron energies[2,3] or of the product ion energy-angle distributions.[4–7] The ionization is associated with intimate encounters where the incoming ground-state potential is generally thought to couple at small internuclear distances, high on the repulsive wall, to excited discrete levels which cross into the continuum and autoionize on the outgoing portion of the trajectory. All of the ionization channels identified have large angular thresholds dictated by the significant repulsive forces at short distances. In contrast, the major ionization channels observed in the present investigation have much smaller angular thresholds than anticipated from a first consideration of the interaction potentials.

APPARATUS

The metastable differential scattering apparatus has been described in detail previously.[8] A beam of fast He^+ ions enters a charge exchange cell filled with Cs. Near-resonant charge transfer produces He atoms predominantly in the 1^1S, 2^1S, 2^1P, 2^3S and 2^3P states, and radiation of the P states leaves a fast neutral beam composed of excited metastable 2^1S, 2^3S, and ground state 1^1S He. The composition of the resulting neutral beam has been estimated theoretically by Olson, Shipsey, and Browne[9] using *ab initio* potential energy curves and close-coupling calculations. They find that the charge-transfer He beam contains 30–35% 2^3S, less than 1% 2^1S, and 65–70% 1^1S in the energy range from 200–400 eV. At lower collision energies, these theoretical calculations are in agree-

ment with experimental evidence[8,10,11] that there is indeed a large ratio of 2^3S to 2^1S metastables. The He^* ions that do not undergo charge transfer are deflected out of the beam before the fast neutrals enter a scattering cell filled with He at pressures low enough to insure single-collision conditions. Scattered particles are detected by two channeltron detectors that can be rotated around the scattering cell. One detector (A) measures the total scattered product intensity as a function of angle and detects both ionic and neutral particles; deflectors between the scattering cell and the detector can remove the ions so that only neutrals are counted, allowing a determination of ionic and neutral product angular distributions separately. The other detector (B) is mounted behind a 127° energy analyzer and can measure the angle-energy double-differential cross section for product ions.

A large exit slot in the target cell allows both detectors, when positioned within the laboratory angular range +75° to −25°, to view the entire intersection of the beam with the target cell. Collimators in front of detector A are used to shield it from background contributions without blocking its view of the interaction region. A collimator at the entrance to the 127° analyzer limits and defines the acceptance solid angle from every position in the interaction region. Both detectors accept a constant solid angle range from every location in the interaction region independent of the angular location of the detector. Hence, there is no "viewing factor" correction needed in comparing the measured intensity at different scattering angles.

Electrostatic deflectors can be used to pulse the original ion beam before it enters the alkali charge-transfer cell. By measuring the difference in flight time to detector A between the original ion beam and the metastable beam and using a separate determination of the ion beam energy with detector B, one can determine the energy of the neutral beam with an accuracy of approximately 0.5 eV. The neutral beam has a lower energy than the parent ions, due mostly to the contact potential of the Cs covered surfaces in the charge-transfer oven.

For analyzing scattered product ion energies, the 127° analyzer is set to transmit a specific ion energy (119 eV in the experiments reported here) with a fixed resolution [measured to be 2.6% (3.1 eV) full width at half maximum (FWHM)]. A few experiments were done with higher-energy resolution, but no additional structure (beyond that reported here) was resolved. Energy scanning is achieved by varying the potential of the entire energy analyzer system. Most of the scattering data were obtained by scanning the product ion energy at a fixed beam energy and laboratory scattering angle. In a typical experiment, a product energy is selected and ions are counted for a specified length of time (e.g., 30 sec). These detected ions include a background produced by collisions of beam metastables with target gas streaming from the scattering cell. By admitting He gas to the main chamber at the same rate that it was previously admitted to the scattering cell, we can determine the background contribution. The floating potential is then varied stepwise to measure both the signal and the background at other product energies. The first point is remeasured occasionally during the course of a scan as a check for variations in beam intensity or scattering gas pressure.

The retardation associated with the floating energy analyzer would be expected to partially defocus the product ions, thereby lowering the counting rate. We compensate for this by a lens in front of the analyzer, adjusted for maximum transmission of the ions with energies corresponding to the peak of the product distribution. The lens voltages were then held constant relative to the analyzer floating voltage. Variations in collection efficiency for ions of different energy have been shown to be small over the energy range of each of the scans presented here. Refocussing the lenses for maximum transmission at every energy in a scan did not increase the intensity at any energy by more than 10% relative to measurements made with constant lens voltages.

In the plane of motion of detector B, the detector angular resolution is calculated to be 0.3° FWHM; the beam profile has a comparable angular width. The angular acceptance perpendicular to the plane of motion of the detector is ±0.5° FW. This out-of-plane window allows scattered particles of larger angle than the nominal apparatus setting to be collected, but the average effect is insignificant at

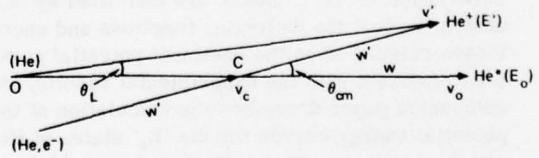

FIG. 1. Kinematic diagram. A beam of He* of laboratory energy E_0 (velocity v_0) is shown colliding with a He target at rest. Laboratory velocities (v_0, v_c, v') are measured relative to the point 0. v_c (= 0.5 v_0) is the velocity of the c.m. Velocities in the c.m. system (w, w') are measured relative to the point C. Primed velocities and energies refer to the product particles. Measurement of E' and θ_L for He^+ specifies w', θ_{cm}, and ΔE (see text).

nominal scattering angles beyond ~1°.

Another source of angular broadening, increasing monotonically with scattering angle but significant only at wide angles, is due to the detector's view of the entire scattering volume 1-mm diam. by 1.25-cm length. At a laboratory angle of 10°, scattering from the entrance and exit regions of the scattering cell is at angles 9.3° and 10.7°, respectively. This broadening does not affect any of the conclusions drawn from the data, although it might decrease the detail observable at the larger scattering angles.

EXPERIMENTS

General remarks

The neutral He beam is a mixture of 2^1S and 2^3S metastables and 1^1S ground state. The least endothermic collisional ionization channels for the three components are, respectively,

$$\mathrm{He}^*(2^1S) + \mathrm{He} \rightarrow \mathrm{He}^+ + \mathrm{He} + e^- - 4.0\ \mathrm{eV}, \quad (1)$$

$$\mathrm{He}^*(2^3S) + \mathrm{He} \rightarrow \mathrm{He}^+ + \mathrm{He} + e^- - 4.8\ \mathrm{eV}, \quad (2)$$

$$\mathrm{He} + \mathrm{He} \rightarrow \mathrm{He}^+ + \mathrm{He} + e^- - 24.6\ \mathrm{eV}. \quad (3)$$

The endothermicities given are for ionization at threshold with ground-state products. For each reaction, the electron can also be ejected with nonzero energy and the product He and He^+ can be formed in excited electronic states.

Figure 1 presents a kinematic diagram and defines some of the symbols to be used in this paper. For product particles of equal mass (neglecting the mass of the electron), an ion detected at laboratory coordinates E', θ_L will correspond to a translational energy loss in the c.m. system of

$$\Delta E \equiv E_{\mathrm{cm}} - E'_{\mathrm{cm}} = 2(E'E_0)^{1/2}\cos\theta_L - 2E'. \quad (4)$$

It is evident that the measured ΔE must equal the sum of the emitted electron energy and the change in internal energy of the heavy particles.

Consider reactions of $\mathrm{He}^*(2^3S)$ as an example. The internal energy of $\mathrm{He}^*(2^3S)$ is 4.8 eV less than the amount required to produce ionic products. Therefore 4.8 eV is the minimum ΔE required to produce ions from reaction (2) and would correspond to zero energy electrons and ground-state products. The first electronically excited product channel is

$$\mathrm{He}^*(2^3S) + \mathrm{He} \rightarrow \mathrm{He}^+ + \mathrm{He}^*(2^3S) + e^- - 24.6\ \mathrm{eV}, \quad (2a)$$

accessible only with measured ΔE values of at least 24.6 eV. Therefore, for ΔE values less than 24.6 eV reaction (2a) is not possible, and only ground-state products are allowed. If $4.8 < \Delta E < 24.6$ eV, the additional endothermicity $\Delta E - 4.8$ eV must reside in kinetic energy E_e of the departing electron. Assuming a pure $\mathrm{He}^*(2^3S)$ beam, there is no ambiguity in product states or electron energies for measured ΔE values in this range. For $\Delta E = 24.6$ eV, reactions (2) and (2a) are both possible, giving 19.8 eV energy either to neutral He product excitation or to the electron translational energy. At higher ΔE values, the entire manifold of He excited states becomes energetically accessible with a limit at

$$\mathrm{He}^*(2^3S) + \mathrm{He} \rightarrow \mathrm{He}^+ + \mathrm{He}^+ + 2e^- - 29.4\ \mathrm{eV}. \quad (2b)$$

Ionization of the ground state component of the beam [reaction (3)] is another possible channel at $\Delta E \geq 24.6$ eV. However, the contributions from (3) can be estimated from the ions produced by scattering a pure beam of ground-state He from a He target. Replacing the Cs charge-transfer vapor with He gas allows resonant charge-transfer production of fast He ground-state beams for these measurements. Data[4,5] for reaction (3) exist at slightly higher energies than our measurements and a comparison of energy loss profiles can be made.

Although the ratio of $\mathrm{He}^*(2^3S)$ to $\mathrm{He}^*(2^1S)$ in the metastable beam is thought to be large,[8-11] contributions from a small component of $\mathrm{He}^*(2^1S)$ might dominate at some values of product energy transfer and scattering angle if the important ionization processes for the two metastables are quite different. Even if the mechanisms were similar for both metastables, the threshold for $\mathrm{He}^*(2^1S)$ ionization might appear at a lower energy because the singlet state is energetically closer to the ionization limit. Since the energetics of reactions (1) and (2) are only 0.8 eV different, the estimated 0.5 eV uncertainty in beam energy makes it unlikely that the effects of the two metastable reactants can be separated upon a first examination of the data. For convenience, we will initially analyze the scattering in terms of the larger 2^3S component of the beam; however, contributions from 2^1S will also be discussed.

Energy distributions

Figure 2 shows an example of a product He^+ ion energy distribution. The data at a metastable beam energy $E_0 = 100.2$ eV and a laboratory scattering angle $\theta_L = 0.0°$ present the measured He^+ distribution plotted versus the laboratory energy E'. In this spectrum, a single feature is observed with a c.m. energy loss ΔE of 4.5 eV. The 0.5 eV uncertainty in beam energy implies that the He^+ ions can be from either reaction (1) or (2) or both; for either reaction, the products are in their

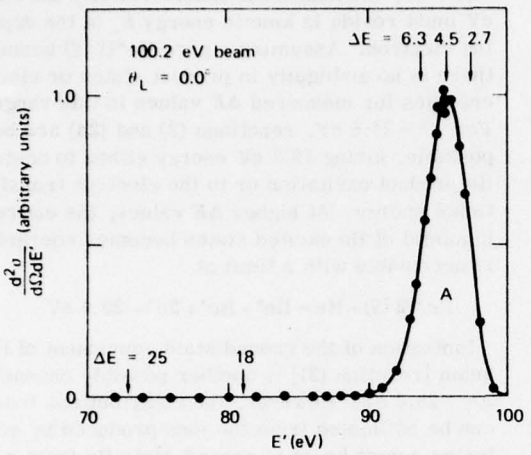

FIG. 2. Distribution of He^+ ions plotted vs product laboratory energy E' for 0.0° scattering of a 100.2 eV He* beam by He. The c.m. collision energy is 50.1 eV; several values of the c.m. endothermicity ΔE are indicated.

ground electronic states and the electron energy is small (<1 eV). There can be no contribution to this feature from ionization of ground-state He in the beam.

The measured energy width of this peak, FWHM = 3.6 eV, is a convolution of the beam energy width, the width due to the distribution of product electron energies, and the width associated with the energy analyzer. The energy analyzer FWHM of 2.6% is 3.1 eV at the 119 eV analysis energy. Hence, the removal of the detector broadening would lower the FWHM to $\sim(3.6^2 - 3.1^2)^{1/2} = 1.8$ eV. The energy width of the original metastable beam is not as easy to ascertain. The beam energy was measured by a time-of-flight (TOF) technique involving a pulsed electric field deflection of the original He^+ ion beam before it was converted by charge transfer to a neutral beam. One major problem with TOF measurement of beam energy width is associated with contributions from the various components of the beam. Each of the He charge-transfer products $1\,^1S$, $2\,^1S$, $2\,^1P$, $2\,^3S$, and $2\,^3P$ has a different energy defect and produces fast neutrals of slightly different energy. The $2\,^1P$ component radiates to become ground-state He($1\,^1S$) which can contribute to the apparent beam energy width but *does not* contribute to the scattered ion peak in Fig. 2. The same argument holds for He($1\,^1S$) formed directly by charge-transfer reactions that yield excited Cs^+ states. The amount of broadening (and shifting) of the measured beam energy due to this component depends on its relative amount and also on whether He*($2\,^3S$) is formed directly or through radiation from He($2\,^3P$). In addition, the act of pulsing the beam can perturb its measured energy distribution from the unpulsed value, usually broadening it somewhat. The result is that the "measured" widths of the neutral beam were variable and usually larger than the 1.8 eV upper limit. Hence, the true energy profile of the metastable beam cannot be obtained from the TOF measurements.

Obviously the ion beam energy width can be used as a lower limit for that of the metastable beam. Measurements with the energy analyzer suggest a width of ~1.0 eV for the parent ion beam. Then the energy width of the emitted electron distribution could be as much as $\sim(1.8^2 - 1.0^2)^{1/2} = 1.5$ eV, but is probably smaller. The uncertainty in beam energy width precludes any serious attempt at deconvoluting the measured energy profiles, but the 3.1 eV FWHM of the 127° energy analyzer is the major source of energy broadening. One can still conclude that the ions observed (Fig. 2) correspond to low energy (<1 eV) electrons having a small (<1.5 eV) spread in energy.

Figure 3 shows representative collisional ionization data at c.m. energy $E_{cm} = 99$ eV ($E_0 \approx 198$ eV). The intensity scale is arbitrary; but the various curves have been normalized to each other by an angular scan that compares the peak intensity from one angle to the next. The data are presented in the laboratory frame without any deconvolution; the measured intensity is proportional to $d^2\sigma/d\Omega dE'$, where $d\Omega$ is a differential laboratory solid angle element. Various values of the c.m. energy loss ΔE calculated from Eq. (4) have been indicated on Fig. 3. At every angle the energy loss profile is dominated by a peak at $\Delta E \approx 5.0$ eV. This component of the He^+ product distribution is labelled "*A*" and will be discussed below. Other prominent features are designated *B*, *C*, and *D* and will also each be described in terms of specific excitation mechanisms. Unlabelled features at large energy-loss values and large angles can have several causes and will only be mentioned briefly.

Figure 4 shows similar representative data at a c.m. energy $E_{cm} = 199$ eV ($E_0 \approx 398$ eV). As in Fig. 3, the intensities are normalized to unity at the peak of the distribution ($\theta_L = 0.0°$, $\Delta E = 5$ eV), and prominent features are labelled for subsequent discussion. The distributions at angles smaller than 1.0° (not shown in Fig. 4) are quite similar at the same value of $\tau = E_0\theta_L$ to the corresponding small angle data at the lower collision energy, although the feature labelled "*D*" is less prominent than it is in Fig. 3.

At 50 eV c.m. energy the scattered signal is significantly smaller than at the higher energies, which causes difficulty in observing any more than the most prominent features. Energy scans at

laboratory angles of 0° (Fig. 2) and 1.2° show only feature "A" with an energy loss peaking at $\Delta E = 4.5$ eV; for angular scans at a fixed $\Delta E = 4.5$ eV, it was possible to follow this feature out to ~5° before it became comparable in size to the background noise.

The laboratory data can be converted to corresponding c.m. differential cross sections through the transformation

$$\frac{d^2\sigma}{d\omega dE'_{cm}} = \frac{w'}{v'}\frac{d^2\sigma}{d\Omega dE'}, \tag{5}$$

where $d\omega$ is the c.m. solid angle volume element, E'_{cm} is the product relative translational energy, and w'/v' can be determined using

$$\frac{w'}{v'} = \left(\frac{E'_{cm}}{2E'}\right)^{1/2} = \left(\frac{E_{cm} - \Delta E}{2E'}\right)^{1/2} \tag{6}$$

and Eq. (4). For the small scattering angles and relatively small energy losses evident in the data considered here, the Jacobian of transformation w'/v' varies by little more than 10% over the entire range of data. Transformation to the c.m. would, for example, decrease the intensity of feature C in Fig. 3 by only about 6% relative to peak A. These changes are comparable to estimates of the uncertainty in peak ratios associated with the energy scanning method used in these experi-

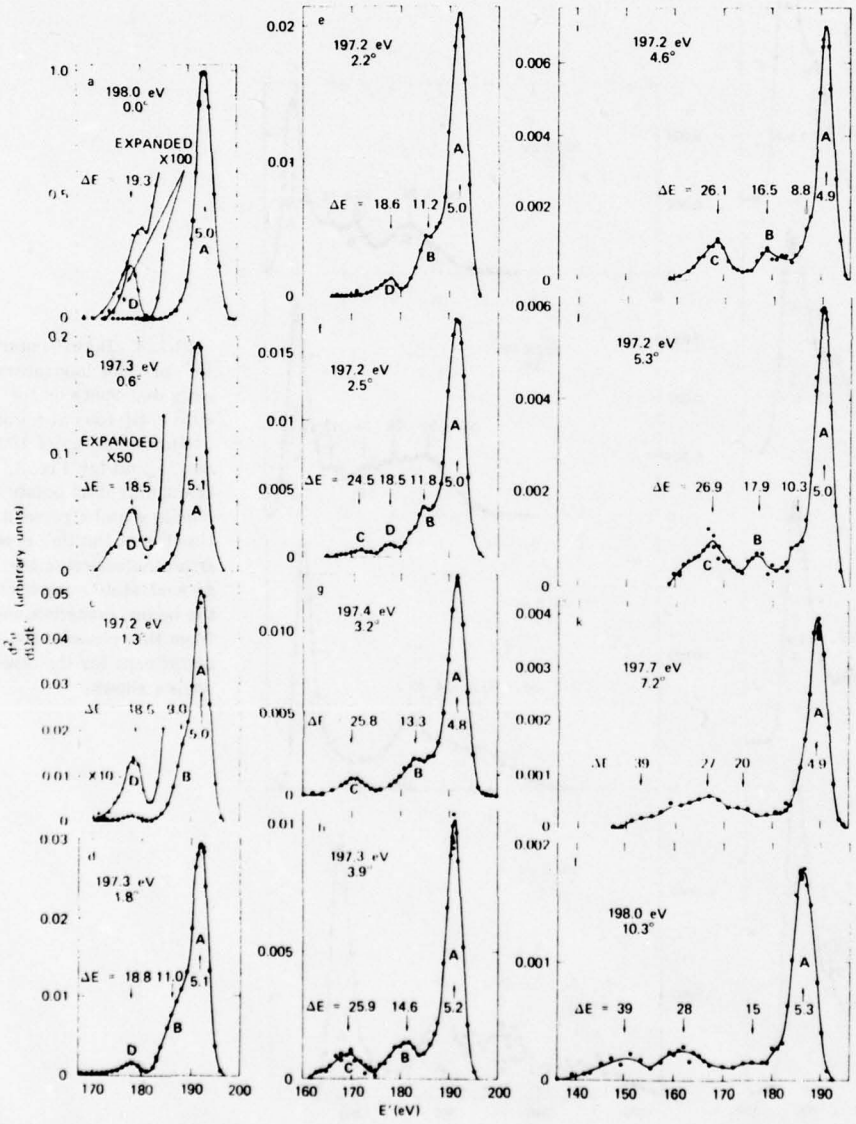

FIG. 3. Representative He^+ product laboratory energy distributions for $He^+ + He$ collisions at a c.m. collision energy of 99 eV. Each spectrum is labelled with the incident beam energy and laboratory scattering angle. All differential cross sections are normalized arbitrarily to unity at the peak of the distribution at 0° using angular normalization data to compare the different angles. Representative values of the c.m. endothermicity ΔE are indicated for each spectrum; the letters A, B, C, and D refer to the ionization features described in the text.

ments (see "Apparatus"), and the two effects should partially compensate.

The c.m. distributions will not be shown directly due to problems associated with presenting the data in that format. As is evident from the kinematics, a particular laboratory angle does not map into a single c.m. angle. Hence, c.m. energy loss distributions at specified angles must be obtained by interpolation of laboratory data, or the c.m. data must be presented as an energy-angle contour map of product intensity. In either case, the large variation in product intensity ($>10^4$) implies that a significantly larger set of data would be needed to produce and to present c.m. results with the clarity of detail possible in Figs. 3 and 4. The existing data are adequate for extracting the essential aspects of the primary ionization processes observed without transforming to the c.m. A rough estimate of the c.m. scattering angle θ_{cm} is its lower limit

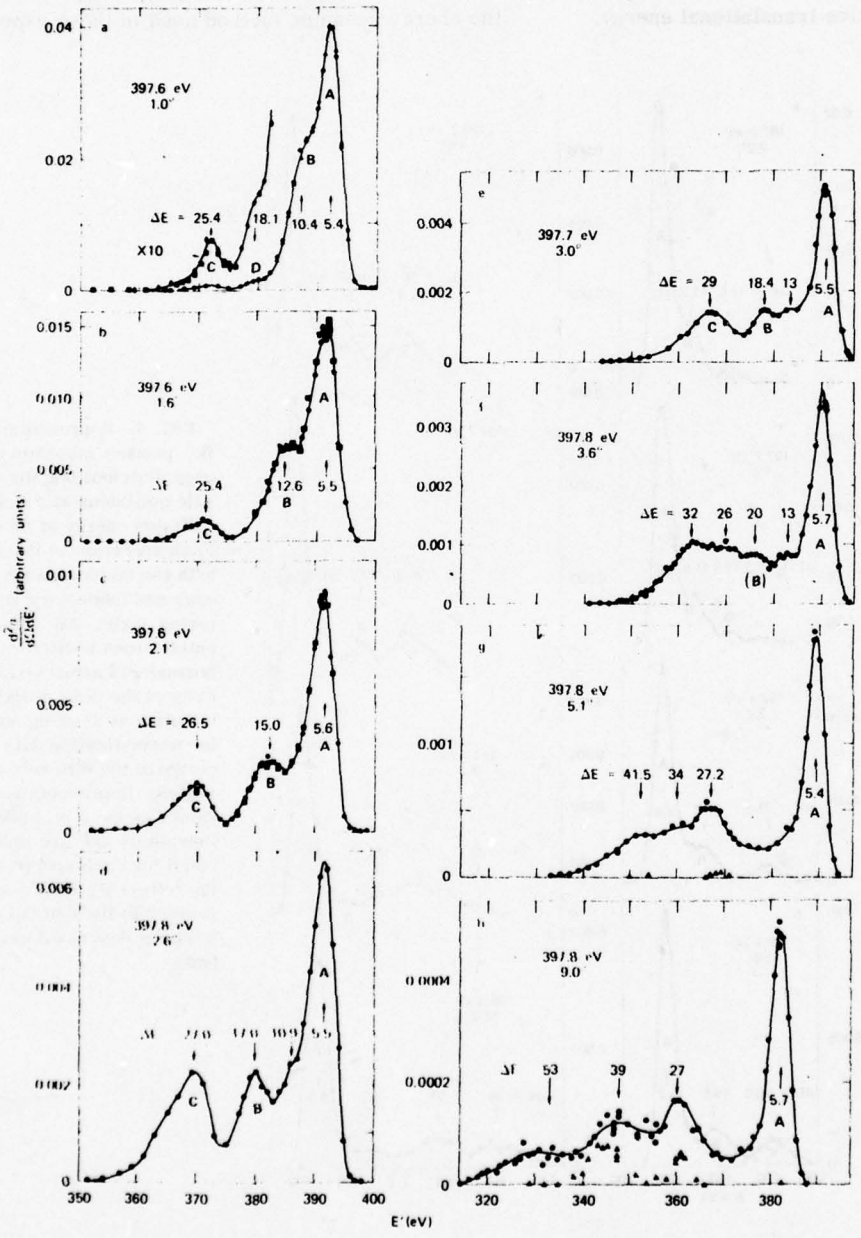

FIG. 4. Representative He' product laboratory energy distributions for He* + He collisions at a c.m. collision energy of 199 eV. See legend for Fig. 3. The triangular data points in panels *g* and *h* present estimates of the He' produced from ionization of the ground-state component of the beam; contributions from this channel are insignificant for the other angles shown.

$$\theta_{cm} \approx 2\theta_L . \tag{7}$$

A more accurate formula for determining θ_{cm},

$$\sin\theta_{cm} \quad (v'/u')\sin\theta_L , \tag{8}$$

involves the same conversion factor used in Eq. (5) for relating laboratory and c.m. differential cross sections. Again for the low-angle scattering and small energy losses measured here, the range in v'/u' is small; in Fig. 3, θ_{cm} would be ~1% and 8% higher than the estimate of Eq. (7) for peaks A and C, respectively, at all angles.

Angular distributions

The angular normalizations referred to above involve measurements of the angular distribution of a specific feature by adjustment of the analysis energy to transmit the peak of the feature at every angle. Our preliminary report[1] on this work presented angular normalization data for peak A at all three collision energies studied. Those distributions (shown in Fig. 5) were used to normalize energy distributions from one angle to another. The angular distributions for all of the other major ionization features are more difficult to determine, since there is only a limited range of angles for which each feature is clearly resolved from other channels. Figure 6 shows an angular normalization for feature C at $E_{cm} = 199$ eV. This reduced c.m. plot of $\rho = \theta \sin\theta\,(d\sigma/d\omega)$ vs $\tau = E_{cm}\theta$ has the threshold behavior characteristic of an inelastic process occurring on a repulsive wall[1-6] and contrasts markedly with the apparent lack of an inelastic threshold seen in the ρ-τ plots for feature A (Fig. 5). Defining the threshold τ_t as the τ value corresponding to half the peak value, one obtains from Fig. 6 a threshold of $\tau_t \approx 725 \pm 25$ eV deg for feature C. The result is the same at $E_{cm} = 99$ eV.

Since feature B first appears at small angles as a shoulder on peak A, its angular dependence is difficult to determine. The rapid decrease in its intensity $d\sigma/d\Omega$ as it shifts to larger ΔE values at larger angles suggests that its angular dependence is qualitatively similar to that of feature A, but no ρ-τ angular threshold can be determined.

Feature D is only observed at small angles, disappearing above $\tau = 600$ eV deg, although it could be masked by the shifting of feature B toward

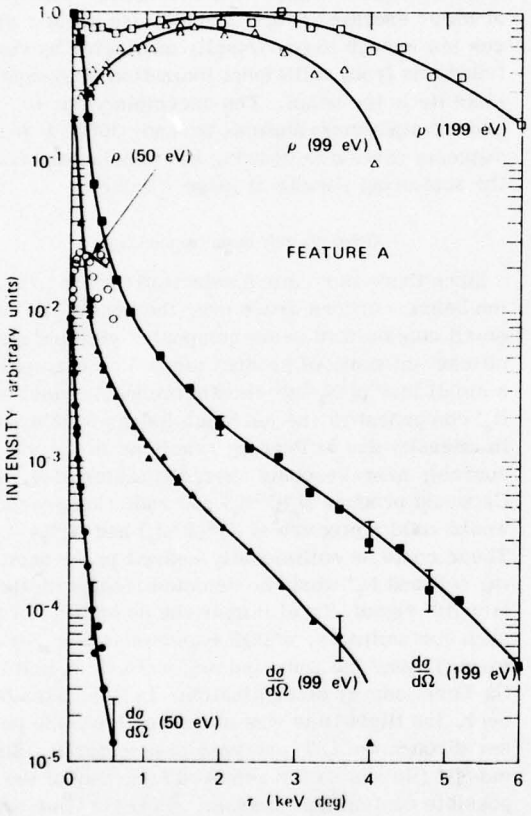

FIG. 5. Experimental angular distributions of the He^+ ions from feature A at an energy loss of ~5 eV. Plotted are the differential cross section $d\sigma/d\Omega$ and the reduced cross sections $\rho = \theta_L \sin\theta_L (d\sigma/d\Omega)$ vs the reduced angle $\tau = E_0\theta_L$ in the laboratory. The analogous c.m. cross sections differ insignificantly. The c.m. energy is indicated for each curve. The intensity units are arbitrary, but the relative intensities for the three energies are approximate values obtained from comparing the ion signal to the beam intensity at each of the energies.

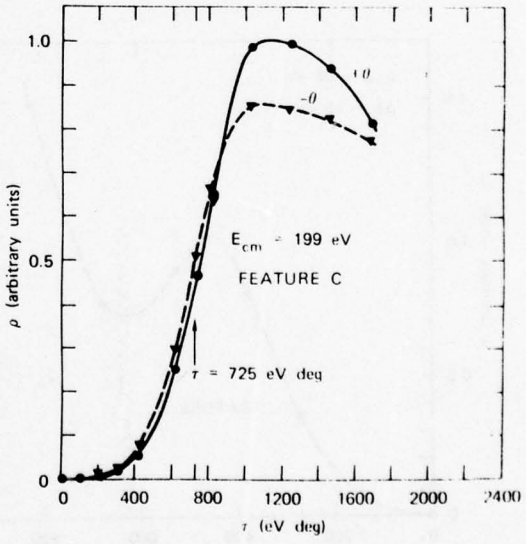

FIG. 6. ρ-τ plot in the c.m. of the experimental angular distribution of the He^+ ions from feature C at E_{cm} = 199 eV. Data points in two directions from the He^+ beam are indicated by the symbols $+\theta$ and $-\theta$.

and through the same energy-loss values. A c.m. angular distribution for an energy loss of 19 eV (corresponding to peak D is shown in Fig. 7 at $E_{cm} = 99$ eV. The measured threshold τ_t is ~310 ± 15 eV deg and the distribution peaks near $\tau = 450 \pm 40$ eV deg. Beyond 600 eV deg the intensity increase is due to the shifting of peak B to higher energy-loss values.

At $\theta_{lab} \gtrsim 10°$, where the intensity was too small for detailed double differential cross section measurements with detector B, supplementary measurements of angular distributions $d\sigma/d\Omega$ were made with detector A. Although these measurements cannot yield detailed information on the product c.m. distribution, they are still useful for estimating the fraction of the total ionization cross section scattered at $\theta_{cm} \gtrsim 20°$ ($\theta_{lab} \gtrsim 10°$ for forward-scattered ions). This is the fraction of the total cross section that has not been examined by energy analysis. At $E_{cm} = 200$ eV this fraction is estimated to be less than 30% of the total cross section. At higher energy the distribution is even more strongly peaked at small angles.

Background due to ground state He in beam

The effect of reaction (3) can be examined most readily by replacing the mixed metastable–ground-state beam by a beam of pure ground-state He. The He beam ($E_0 = 398$ eV) was produced by resonant charge transfer in a charge-exchange cell

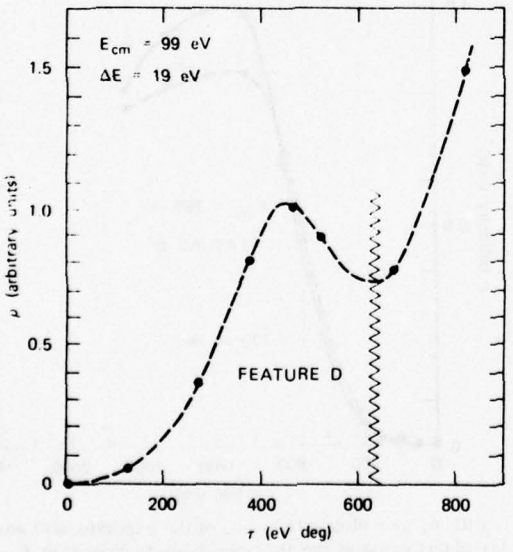

FIG. 7. ρ-τ plot in the c.m. of the experimental angular distribution of the He^+ ions at $\Delta E = 19$ for E_{cm} 99 eV. Feature D appears at small τ values; beyond ~600 eV deg, other processes contribute at this ΔE value.

filled with He gas and scattered and detected under identical conditions to those for the metastable beam. Two energy profiles for reaction (3) are included in Fig. 4 (panels g and h) for laboratory scattering angles of 5.1° ($\tau = 2030$ eV deg) and 9.0° ($\tau = 3600$ eV deg). The normalization of the results to the mixed metastable-ground-state beam used in Fig. 4 is based on an estimated He/He* ratio of 2 : 1 in the metastable beam.[9] The shape of this distribution is quite comparable to profiles obtained by Brenot *et al.*[5] under similar conditions.

Clearly the ground-state contribution at 9° (3600 eV deg) is quite substantial for large values of ΔE. The contribution at 5.1° ($\tau = 2030$ eV deg) is small (certainly less than 10% at all values of ΔE), and at even smaller angles it is negligible. The data at lower energies (Figs. 2 and 3) are all at τ values low enough to be virtually unaffected by contributions from collisional ionization of ground-state He in the beam. The uncertainty due to ground-state contributions beyond ~3000 eV deg suggests caution in drawing any conclusions from the scattering results at large τ values.

Other possible beam contaminants

Since there is no mass selection for the primary ion beam, concern arose over the possibility of a small contaminant beam component yielding significant intensity of product ions. For example, a small leak of N_2 into the source would yield an N_2^+ component in the ion beam (perhaps enhanced in intensity due to Penning reactions in the ion source); near-resonant charge transfer of N_2^+ with Cs would produce $N_2(C\,^3\Pi_u)$ and radiation cascade would yield a mixture of $N_2^*(B\,^3\Pi_g)$ and $N_2^*(A\,^3\Sigma_u^+)$. These could be collisionally ionized in the scattering cell and N_2^+ would be detected along with the true He^+ signal. To eliminate the possibility of any such contaminants, a TOF experiment was performed using the same pulsing method applied to the beam energy determination. In this case, however, the flight time was measured from the pulser through the 127° analyzer to detector B. Since mass 4 (He^+) is so far removed from any of the possible contaminant masses, its flight time was easy to resolve and identify. This method of simultaneously determining the velocity and energy of an ion was used to verify that each of the four major ionization features (A, B, C, D) was due to mass 4 (He^+); no significant contamination of the results with other masses was observed.

Other ionic products

The associative ionization reaction

$$He^* + He \rightarrow He_2^+ + e^- \qquad (9)$$

is less endothermic than reactions (1) and (2) and might contribute to the reaction cross section at low energies. However, at the energies considered here, the electron must remove considerable energy to stabilize the product ion; and associative ionization is unlikely. Since the He_2^+ product ions are expected to have "exactly" the velocity of the center of mass, one can collect any products efficiently at an analysis energy of half the incident beam energy and an angle of 0°. We could detect no evidence of associative ionization in these experiments.

Another possible reaction produces the stable $He^-(1s2s2p)^1P$ ion[12] through

$$He^*(2\,^3S) + He(1\,^1S) \rightarrow He^+(^2S) + He^-(^4P) - 24.5\ \text{eV}. \quad (10)$$

The energy loss of 24.5 eV confines any fast He^- (i.e., He^- produced in the forward direction corresponding to slow He^+ product) to a specific velocity at every scattering angle. With a 398 eV He^* beam a search for He^- was made but no convincing evidence of its presence was obtained. We concluded that reaction (10) could contribute no more than a very small fraction of the He^+ signal seen at $\Delta E \approx 25$ eV.

DISCUSSION

As mentioned previously, we will initially concentrate our attention on $He^*(2\,^3S)$ because it is predicted to be a much larger fraction of the beam than $He^*(2\,^1S)$; effects possibly due to the $He^*(2\,^1S)$ component will become apparent as we proceed in the discussion.

The interpretation of the $He^*(2\,^3S) + He(1\,^1S)$ collisional ionization data requires not only a knowledge of the potential energy curves for the $He^*(2\,^3S) + He$ system, but also a knowledge of the various potential curves for the $He^+ + He$ system. In order to understand these processes, we utilize the He_2^* and He_2^+ potential energy curves shown in Fig. 8. The $^3\Sigma_g^+$ adiabatic potential of He_2^* is taken from the work of Lenamon *et al.*,[13] and the $^3\Sigma_g^+$ diabatic potential is from the paper by Evans *et al.*[14] with an exponential extrapolation in the repulsive region. The $^2\Sigma_g^+$ and $^2\Sigma_u^+$ potentials of He_2^+ are from the work of Marchi and Smith[15] with the well depth of the $^2\Sigma_u^+$ state increased slightly to agree with the more accurate results of Liu.[16] The $^2\Sigma_g^+$ potential curve of $He^+ + He^*(2\,^3S)$ is obtained from an analysis of inelastic scattering data.[17]

Given this available potential energy curve information,[18] we can calculate the deflection functions[19] for several possible mechanisms for each ionization process observed experimentally. Then, by comparing the observed and calculated angular thresholds, energy losses, and cross-section behavior, we can appraise the success of various proposed mechanisms at reproducing the experimental results.

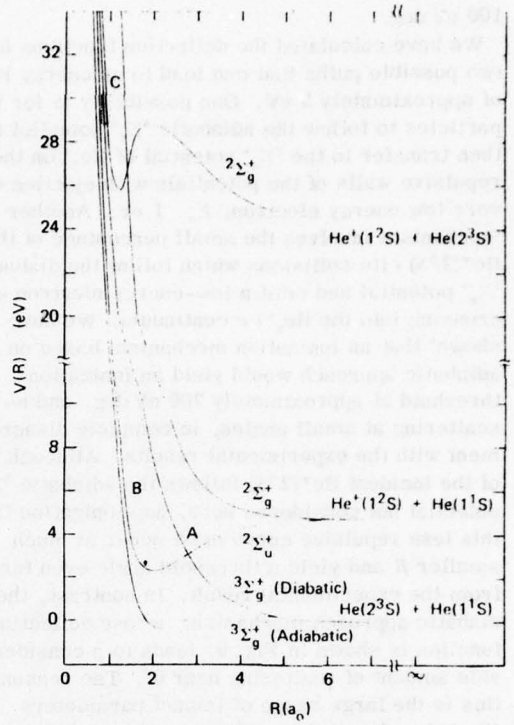

FIG. 8. Several of the He_2^* and He_2^+ potential curves useful for a description of ionization in $He^*(2\,^3S) + He$ collisions. Sources for curves: adiabatic $^3\Sigma_g^+$ from Lenamon *et al.* (Ref. 13); diabatic $^3\Sigma_g^+$ from Evans *et al.* (Ref. 14) with an exponential extrapolation at small R; $^2\Sigma_u^+$ and repulsive $^2\Sigma_g^+$ from Marchi and Smith (Ref. 15) with the well depth adjusted to Liu's value (Ref. 16); and upper $^2\Sigma_g^+$ from Olson (Ref. 17). The $^3\Sigma_u^+$ curve correlating asymptotically to $He^*(2\,^3S) + He(1\,^1S)$ is not shown; half of the incoming $He^*(2\,^3S)$ metastables follow this potential.

We will divide the theoretical interpretation into several parts, each of which is concerned with a specific feature of the collisional ionization of $He^*(2\,^3S)$.

Process A

The most prominent ionization mechanism yields a peak of high intensity found at a ΔE of approximately 5 eV associated with ground-state ion products and very-low-energy electrons. This peak has an extremely large intensity and more surprisingly, is found at very small scattering angles, peaking at 0°. If there is an angular threshold in the ρ-τ plots (Fig. 5), it must be at τ values below

100 eV deg.

We have calculated the deflection functions for two possible paths that can lead to an energy loss of approximately 5 eV. One possibility is for the particles to follow the adiabatic $^3\Sigma_g^+$ potential and then transfer to the $^2\Sigma_u^+$ potential of He_2^+ on the repulsive walls of the potentials with ejection of a very low energy electron, E_e 1 eV. Another mechanism involves the small percentage of the He*($2\,^3S$) + He collisions which follow the diabatic $^3\Sigma_g^+$ potential and emit a low-energy electron upon crossing into the $He_2^+ + e$ continuum. We have shown[1] that an ionization mechanism based on the adiabatic approach would yield an ionization threshold at approximately 700 eV deg, and no scattering at small angles, in complete disagreement with the experimental results. Although half of the incident He*($2\,^3S$) follows the adiabatic $^3\Sigma_u^+$ potential not considered here, any ionization from this less repulsive curve must occur at much smaller R and yield a threshold angle even further from the experimental result. In contrast, the diabatic approach mechanism, whose deflection function is shown in Fig. 9, leads to a considerable amount of scattering near 0°. The reason for this is the large range of impact parameters ($b \approx 1.7a_0$–$2.8a_0$) contributing to the small angle scattering as seen in Fig. 9, and the fact that the intensity at small angles is further accentuated by an inelastic rainbow effect due to the minimum on the diabatic deflection function. The attractive forces on the $^2\Sigma_u^+$ ion curve essentially compensate for the repulsive forces on the incoming diabatic state, resulting in small overall deflection angles. Hence, it appears that the dominant ionization mechanism occurs through a diabatic channel.

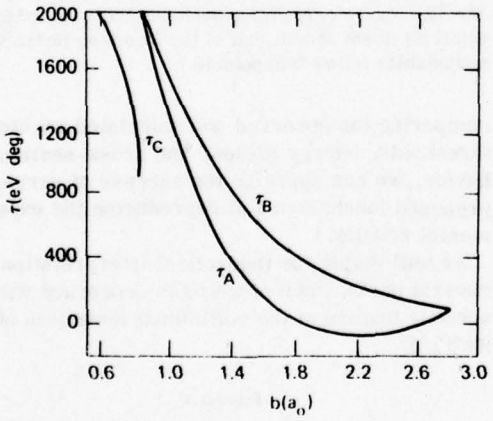

FIG. 9. Deflection functions vs impact parameter calculated for collisions following the $^3\Sigma_g^+$ diabatic potential shown in Fig. 8. For τ_A, ionization occurs at the first crossing into the continuum at point A in Fig. 8; τ_B is the deflection function obtained when ionization occurs at the classical turning point and the products separate on the ground-state ion curve; τ_C is calculated assuming transfer to the excited $^2\Sigma_g^+$ ion curve in region C of Fig. 8.

We can estimate the percentage of the particles that follow the diabatic $^3\Sigma_g^+$ potential into the continuum by using the transition probabilities calculated by Evans *et al.*[14] for the reaction He*($2\,^3S$) + He – He($2\,^3P$) + He. This is a single transition from the lowest to the next highest adiabatic $^3\Sigma_g^+$ potential curve. Following the diabatic $^3\Sigma_g^+$ potential into the continuum can be viewed as involving a series of such transitions between successively higher and closer-spaced adiabatic curves. The spacing between the first two adiabatic curves is much larger than the other spacings, implying that the transition probability into the continuum is not very different from the value for this first crossing. The close-coupled transition probabilities of Evans *et al.*[14] can be used to obtain the jumping probability from $2\,^3S$ to $2\,^3P$ in a single crossing of the region of mixing. For impact parameters near the inelastic rainbow this probability is a few tenths of a percent at a c.m. collision energy of 50 eV and 2–5% in the energy range from 100 to 200 eV. The coupling matrix elements calculated by Cohen[20] for the higher crossings can be used in a Landau-Zener treatment to estimate that the overall probability for continuing diabatically into the continuum is ~50–90% of the $2\,^3S - 2\,^3P$ probabilities in this energy range. Hence, the overall transition probabilities are substantial and increase by approximately an order of magnitude from 50 to 200 eV. This is in good qualitative agreement with the estimated experimental energy dependence, obtained from a normalization of product ion signals at the three energies (Fig. 5).

A schematic molecular orbital correlation diagram for He + He collisions is shown in Fig. 10. In a molecular orbital picture[21] the diabatic $^3\Sigma_g^+$ state has $1s\sigma_g 2p\sigma_u^2 2s\sigma_g$ character at small R and the ionization involves a two-electron transition to the ionic state $1s\sigma_g^2 2p\sigma_u$ and a free electron. One electron drops down to fill the vacancy in the lowest molecular orbital while another is promoted into the continuum.

The small component of He*($2\,^1S$) in the beam has an analogous diabatic $^1\Sigma_g^+$ path into the continuum. The diabatic $^1\Sigma_g^+$ potential and the low-lying adiabatic $^1\Sigma_g^+$ potentials have been calculated by Guberman and Goddard.[22] The major relevant difference between the $^1\Sigma_g^+$ and $^3\Sigma_g^+$ potentials for a comparison of overall probabilities for proceeding diabatically into the continuum involves a smaller splitting in the $^1\Sigma_g^+$ case between the incoming ($2\,^1S$) and the next highest ($2\,^1P$) adiabatic curve. Close-coupled transition probabilities are

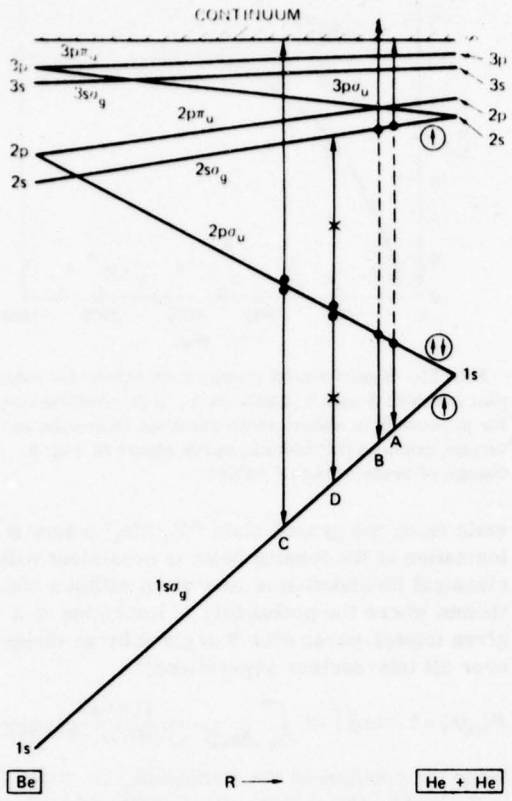

FIG. 10. Molecular orbital correlation diagram for Be ⇌ He + He showing schematically the lowest orbitals. The orbitals are labelled in united atom nomenclature. The circled arrows at the right represent the electrons in the configuration $1s\sigma_g 2p\sigma_u^2 2s\sigma_g$ corresponding to the incoming diabatic $^3\Sigma_g^+$ molecular potential. The singlet case is similar. The vertical arrows labelled *A*, *B*, *D*, and *C* show the two-electron transitions associated with the processes described in the text. Process *D* is not possible for the triplet component of the beam, but is observed for singlet metastables approaching along the diabatic $^1\Sigma_g^+$ potential; the transition $1s\sigma_g 2p\sigma_u^2 2s\sigma_g \rightarrow 1s\sigma_g^2 2s\sigma_g^2$ is followed by ionization at large distances.

not available for the $(^1\Sigma_g^+)$He*$(2\,^1S)$ + He → He$(2\,^1P)$ + He excitation, but the smaller splitting[23] implies a much greater transition probability, with a magnitude of roughly 20–50% in the c.m. energy range 50–200 eV.

The ratio of He*$(2\,^3S)$ to He*$(2\,^1S)$ in the beam is estimated theoretically to be ~30–50 in this energy range.[9] Comparing the estimated beam ratios and estimated transition probability ratios for the two metastable components of the beam suggests that the contribution of the He*$(2\,^1S)$ metastable to the collisional ionization may be substantial, especially at $E_{cm} = 50$ eV where the transition probability along the diabatic $^3\Sigma_g^+$ potential becomes quite small.

Since the beam composition and diabatic transition probabilities are only theoretical estimates with no experimental confirmation, the relative contribution of He*$(2\,^1S)$ to the ionization can only be crudely estimated; and there is no easy way to separate the two contributions experimentally. The difference in initial energy of 0.8 eV between the two levels implies that the deflection function for ionization of the He*$(2\,^1S)$ should be slightly less repulsive than the calculated result for the $2\,^3S$ component (Fig. 9) and that the energy loss values should be lower by 0.8 eV. It should be noted that as the c.m. energy varies from 50 to 200 eV the measured energy loss of peak *A* varies from 4.5 ± 0.5 to 5.5 ± 0.5 eV, consistent with the suggested decrease in the He*$(2\,^1S)$ contribution with increased energy. However, another effect can be responsible for this shift, an increase in the emitted electron energy with increased collision energy due to quicker transit into the continuum.[2,3] Other strong evidence for contributions of He*$(2\,^1S)$ to the observed ionization exists in our observation that process *D* is due entirely[23] to the singlet component of the beam; clearly, the He*$(2\,^1S)$ contribution to other ionization features, including feature *A*, cannot be discounted.

Our description of process *A* has so far been limited to a single channel even though other contributions to ionizations with an energy loss of ~5 eV are possible. For example, one can follow the diabatic $^3\Sigma_g^+$ (or $^1\Sigma_g^+$) curve all the way to the turning point and ionize on the *outgoing* trajectory near the crossing out of the continuum. This process involves a larger amount of repulsive interaction and should not contribute to the intense forward scattering. However, if a significant fraction of the incoming flux can reach and return from the inner turning point without suffering autoionization, this channel might contribute to feature *A* at larger τ values.

Consider further the case where the outgoing flux continued down through the continuum crossing without autoionizing. Since the original probability of following the diabatic $^3\Sigma_g^+$ curve into the continuum was small, the chance of returning elastically must also be small. This could lead to excitation of excited states lying between the incoming level and the continuum. Among these are excited ionic states of the form $He^+ + He^-(1s^2nl)$. Although, to our knowledge, there is no evidence for $He^-(1s^2nl)$ states, they may exist in the field of a He^+, yielding potentials that are Coulombic at large distances and are asymptotically above the $He^+ + He$ continuum. Barat and co-workers[4,5] have invoked such states to explain similarities in excitation and ionization channels for ground-state He-He

collisions. If these states are populated on the outgoing leg of the trajectory, they will cross into the continuum at large distances, yielding a low energy electron and contributing to process A. The Coulombic attraction can compensate for the earlier repulsion to produce low angle scattering and an inelastic rainbow. Another possibility involves collisions following the adiabatic $^3\Sigma_g^+$ (or $^1\Sigma_g^+$) potential to the turning point, then making a transition (diabatic) to a $He^+ + He^-$ potential on the outgoing trajectory. In either case the Coulombic exit channel must pass diabatically with little interaction at large distances through a manifold of excited neutral states of the same symmetry if the continuum is to be reached.

In a companion paper, Saxon *et al.*[23] calculate the lowest $^1\Sigma_g^+$ potential curves of He_2 formed from 1*s* and 2*s* electrons. There are two singly excited $^1\Sigma_g^+$ curves associated with $He^*(2\,^1S) + He(1\,^1S)$ and $He^+ + He^-(1s^2 2s, 2\,^2S)$, respectively, at large distances. The repulsive diabatic $^1\Sigma_g^+$ potential has the character of the $He^* + He$ adiabatic curve at large distances and resembles the $He^+ + He^-$ adiabatic potential at smaller R.

At present, evidence for possible contributions to process A from large distance autoionization along a Coulombic $He^+ + He^-$ potential are rather difficult to separate from the mechanism proposed. Other ionization features discussed below demonstrate directly the importance of the repulsive diabatic potential, whereas evidence of the long-range autoionization comes indirectly from other experimental results on the He + He system.[4,5] The various possible contributions to feature A for each metastable should interfere coherently, and any oscillations, if they were to be observed, could possibly be identified with specific channels. Unfortunately, the oscillation patterns might be washed out, since there are several possible important interfering channels for two different incident metastables.

Process *B*

One of the most interesting observations is an energy loss that changes with angle and collision energy but is well correlated with the reduced angle $\tau = E\theta$ (see Fig. 11). This implies that the energy-loss process depends directly on the impact parameter. The observed energy losses increase with increasing τ and vary from approximately 9 to 20 eV, with values outside this range possibly obscured by overlap with other ionization features. This behavior can be ascribed to a collision in which the system follows the diabatic incoming channel until it reaches the classical turning point R_0, ionizes at the turning point, and

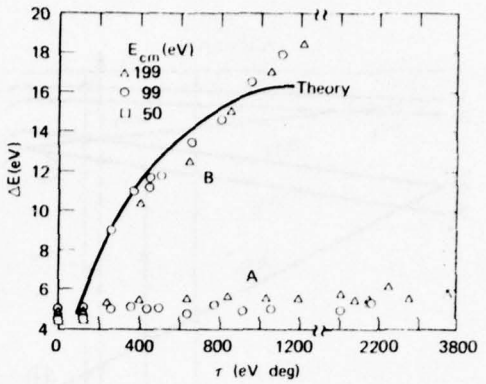

FIG. 11. Experimental energy loss values for ionization features A and B plotted vs τ. A theoretical curve for process B is shown which assumes ionization at the turning point on the diabatic curve shown in Fig. 8. Note change of scale at high τ values.

exits along the ground state $(^2\Sigma_u^+)He_2^+$ potential. Ionization at the turning point is consistent with a classical formulation of ionization within a continuum where the probability of ionization at a given impact-parameter b is given by an integral over all internuclear separations[24]

$$P_{\text{ion}}(b) = 1 - \exp\left(-2\int_{R_0}^{\infty} \frac{\Gamma(R)\,dR}{\hbar v_0 [1 - V(R)/E - b^2/R^2]^{1/2}}\right).$$

Since the coupling to the continuum, the width Γ, is divided by the radial velocity before integration, autoionization of the molecular state formed during the collision should have a peak at the distance of closest approach where the radial velocity is zero.

To demonstrate this effect for $He^*(2\,^3S)$ collisions, we calculated a deflection function using the diabatic $^3\Sigma_g^+$ potential and the $^2\Sigma_u^+$ ion potential (similar results would be obtained with incident $He^*(2\,^1S)$ metastables). The result is plotted as τ_B in Fig. 9. Corresponding energy-loss values were determined from the potential differences at the turning point and are plotted along with the experimental data for feature B in Fig. 11. The agreement is quite good except at the large τ values corresponding to small R_0 where the potential curves are strongly repulsive. Here the energy loss is strongly dependent on slight changes in the relative slopes of the two curves; since the calculated curves are essentially parallel, the predicted energy-loss values become constant.

Consideration of the molecular orbital characters of the two relevant potential curves, however, suggests that the "true" potentials continue to separate as the turning point decreases and that the extrapolation of the $^3\Sigma_g^+$ diabatic curve at small distances should be higher than shown in Fig. 8. Above the continuum crossing, the $^3\Sigma_g^+$ diabatic

potential can be characterized by the configuration $1s\sigma_g 2p\sigma_u^2 2s\sigma_g$, while the ground-state $^2\Sigma_u^+$ ion potential has a $1s\sigma_g^2 2p\sigma_u$ configuration in the same region. The difference potential should be dominated by the extra antibonding $2p\sigma_u$ electron in the $^3\Sigma_g^+$ potential and the extra bonding $1s\sigma_g$ electron in the ion curve. Actually, the $^3\Sigma_g^+$ diabatic potential should be more nearly parallel at small R to the $^2\Sigma_g^+$ ion curve whose configuration $1s\sigma_g 2p\sigma_u^2$ is different only in the relatively small effect of the $2s\sigma_g$ electron. Hence, a better value for the potential at small R should yield an energy loss for process B which continues to increase with τ, in agreement with the experimental data. The ionization process is again a two-electron transition from $1s\sigma_g 2p\sigma_u^2 2s\sigma_g$ to $1s\sigma_g^2 2p\sigma_u + e^-$, as indicated schematically in Fig. 10.

The experimental data (Figs. 3 and 4) contain strong evidence of secondary structure developing between peaks A and B at large angles [Figs. 3(i), 3(j), 4(d)–4(f)]. The most convincing evidence is obtained from the similarities in this secondary structure at different energies when they are compared at the same τ value, e.g., Figs. 3(j) and 4(d). This structure can be understood by considering the consequences of the fact that the ionization does not occur exclusively at the turning point.

All scattered ions from process B found at a specified energy loss ΔE_1 correspond to a single internuclear distance R_1 at which the electron emission occurs. The largest intensity is associated with collisions whose turning point is precisely R_1, but collisions with smaller impact parameters can ionize at R_1 either on the incoming or the outgoing leg of their trajectories. For the specified energy loss ΔE_1, one can represent the heavy particle interactions by translating the $^2\Sigma_u^+$ ion curve upwards so that it intersects the incoming diabatic curve at R_1. Then it is easy to see that interference between ionization on the incoming and outgoing legs of the trajectory yields Stückelberg oscillations in the angular distribution equivalent to those observed in a two-state inelastic scattering problem.[25] At other energy-loss values the angular distribution will have similar interference structure, but will be shifted in the same way that the angular distribution of feature B shifts with energy (Fig. 11).

This structure in both angle and energy is probably responsible for the secondary oscillations observed in the data. No quantitative analysis of this effect will be attempted since the quality of the data does not warrant it. An analysis by Sidis[26] of a similar effect observed by Barat *et al.*[27] for the reaction

$$He^+ + He \rightarrow He^{+*} + He + e^-$$

demonstrates, however, that the mechanism proposed here is a reasonable way of explaining the structure.

Process D

The combination of small scattering angles coupled with large energy losses (18.7 ± 0.5 eV) for peak D causes some difficulty in producing a reasonable explanation of the process involved. There appears to be no realistic ionization mechanism involving He*($2\,^3S$) that would produce such a result. However, for the He*($2\,^1S$) metastable, radial coupling of the incoming $^1\Sigma_g^+$ diabatic state with the doubly excited $^1\Sigma_g^+$ state dissociating to He*($2\,^3S$) + He*($2\,^3S$), followed by molecular autoionization at large distances on the doubly excited curve, would yield an energy loss of 19.0 eV. Yet, it is not immediately clear why this doubly excited curve would be favored over all the similar higher-energy states and why the scattering would be found at such low angles.

A companion paper[23] presents an *ab initio* calculation of the relevant $^1\Sigma_g^+$ excited He_2 potentials, verifies the existence of a crossing between the incoming diabatic potential and a deep inner well in the doubly excited He_2 potential, and demonstrates that an inelastic rainbow effect can produce low angle scattering into this channel. The crossing from the incoming diabatic potential to the doubly excited $^1\Sigma_g^+$ curve involves the two-electron transition from $1s\sigma_g 2p\sigma_u^2 2s\sigma_g$ to $1s\sigma_g^2 2s\sigma_g^2$ (see Fig. 10). The existence of molecular autoionization at large distances on this exit channel potential has already been demonstrated in ground-state He-He collisions by Gerber *et al.*[3]

Process C

Another prominent inelastic process is characterized by an energy loss of approximately 25–27 eV which has a broad threshold with a half-rise point at $\tau = E\theta \approx 725$ eV deg. The τ threshold is constant as the collision energy is varied which implies that the mechanism for the production of this channel involves a curve crossing[25] (i.e., not rotational coupling in the united atom limit). This energy loss seems consistent with reaction (2a) and can be readily understood by referring to the potential energy diagram shown in Fig. 8. At small internuclear separations, the diabatic $^3\Sigma_g^+$ potential energy curve of He_2^* approaches the excited ionic $^2\Sigma_g^+$ potential curve arising from $He^+ + He^*(2\,^3S)$. If in the interaction region labeled C a low-energy electron is ejected, an ionization process with an energy loss of ~25 eV would be observed (reaction 2a). It is possible to estimate the angular threshold for this energy

loss process from a deflection function analysis. From calculations using the potential curves in Fig. 8, we estimate a threshold of approximately 900 eV deg. The calculated deflection function is labelled τ_c in Fig. 9. In a discussion of process *B* above, it was noted that the diabatic $^3\Sigma_g^+$ potential is probably more repulsive at small distances than shown in Fig. 8. This would move the coupling region *C* to larger *R* values and should shift the threshold for process *C* to smaller τ values.

Near the threshold for process *C*, the energy loss value ΔE is ≈ 25 eV, implying a very-low-energy for the emitted electron. At scattering angles above the threshold, the energy loss value shifts gradually from 25 to ~27–29 eV. There are two obvious possible causes of the shift: ion production accompanied by population of the set of higher neutral states whose asymptotes lie between those of reactions (2a) and (2b); or an increasing energy of the emitted electron accompanying the larger scattering angles. A consideration of the molecular orbitals indicates that excitation of a higher neutral state is unlikely, since reaction (2a) involves the two-electron transition (shown in Fig. 10)

$$1s\sigma_g 2p\sigma_u^2 2s\sigma_g \rightarrow 1s\sigma_g^2 2s\sigma_g + e^- ,$$

whereas higher excitation must involve additionally a promotion of the $2s\sigma_g$ electron, yielding three-electron transitions of much lower probability.

Another possible contribution to feature *C* is from excited Coulombic states correlating asymptotically to $He^+ + He^{-*}$. There is more compelling evidence for the doubly excited He^- states $1snln'l'$ than for the $1s^2nl$ states discussed with relation to feature *A*. They have been seen as electron scattering resonances,[28] and have been utilized in explaining various structure in the electron spectra from He-He collisions.[2-4] From the incoming diabatic state, two-electron transitions can populate molecular orbitals of the form $1s\sigma_g^2 2s\sigma_g n\sigma$ leading to the possible asymptotic population of $He^+ + He^-(1s2snl)$ states. Autoionization at large distances on these states can produce energy losses compatible with feature *C*. Coulombic attraction on the outgoing leg of the trajectory could lower the angular threshold for one or more of these $He^+ + He^-$ channels below that calculated for reaction (2a). The best candidate for low angle scattering would involve first a transition to the $1s\sigma_g^2 2s\sigma_g^2$ excited state, followed by a separation along the $He^+ + He^-$ $(1s2s^2)$ potential rather than the adiabatic $He^*(1s2s) + He^*(1s2s)$ curve important to process *D*. Without *ab initio* calculations of the $He^+ + He^-$ excited potentials it is difficult to assess the importance of these states.

Other processes

Other ionization channels can open up for smaller impact-parameter collisions and larger scattering angles. Examination of a Lichten[21] type correlation diagram (Fig. 10) demonstrates, for example, the importance of rotational coupling in the united atom limit of the $2p\sigma_u$ and $2p\pi_u$ molecular orbitals. This coupling is important for collisions following the $^{1,3}\Sigma_u^+$ and $^{1,3}\Sigma_g^+$ adiabatic potentials as well as the diabatic curve. The resultant $1s \rightarrow 2p$ transitions can produce $He(2s2p) + He$ and higher excitations. Autoionization at large separations of the doubly excited He^{**} states will yield energy losses near ~40 eV. Structure at large τ values may be due to this mechanism, but the data are not of sufficient quality to warrant a more detailed examination. Also, contributions from the ground-state component of the beam become important in the same region of τ and energy loss.

It is worth noting that, except for degeneracies in the united atom limit, there are no important contributions to collisionsal ionization associated with crossings of molecular *orbitals*. Transitions to excited states at the normally important crossing of the attractive $2s\sigma_g$ orbital with the repulsive $2p\sigma_u$ must involve two-electron transfer to conserve the *g* or *u* character of the incoming state; yet the incoming configurations $1s\sigma_g^2 2p\sigma_u 2s\sigma_g$ $(^{1,3}\Sigma_u^+)$, $1s\sigma_g^2 2p\sigma_u 3p\sigma_u$ $(^{1,3}\Sigma_g^+$ adiabatic), and $1s\sigma_g 2p\sigma_u^2 2s\sigma_g$ $(^{1,3}\Sigma_g^+$ diabatic) all do not allow this possibility. Two-electron transitions occur at crossings of molecular states or in the continuum, not at crossings of molecular orbitals. This restriction is not in effect for ground-state He-He collisions where the $2p\sigma_u^2 \rightarrow 2s\sigma_g^2$ transition[2-4] produces significant excitation, e.g.,

$$He + He \rightarrow He^*(1s2s) + He^*(1s2s) .$$

Expected electron energy distributions

Our analysis of the collisional ionization mechanisms can be used to estimate qualitatively the electron energy distribution expected from these reactions. Clearly, the major peak in the electron energy distribution would be from process *A* with electrons having an energy below ~1 eV. Process *B* and its interference structure would produce a broad continuum of electron energies extending from peak *A* to higher energies. Feature *C* would again yield low-energy electrons (a few eV or lower) and possibly a peak at 19.3 eV if autoionization from the $He^+ + He^-$ $(1s2s^2)$ potential contributes. Feature *D* would produce ~15 eV electrons from the molecular autoionization although the total intensity might be small relative to the intense continuum distribution from process *B*

that underlies it. The He($2s2p$) autoionizing state mentioned briefly would eject an electron with energy near 35 eV.[2,29]

It must, of course, be emphasized that up to 30% of the total cross section for ion production at $E_{cm} = 199$ eV occurs with c.m. scattering angles above ~20°. The lack of detailed differential scattering data at these angles implies that other mechanisms could contribute substantial electron intensities at energies different from those predicted here.

Recently, product electron energy distributions have been measured for this reaction[10,30] over a similar energy range. Such measurements have inherently higher resolution and can identify some of the highly excited product channels, but there are experimental difficulties associated with detection of the low-energy electrons.[30]

Total cross sections

If, as we conclude, ionization occurs predominantly for collisions following the diabatic incoming potential, we can estimate the total cross section for ionization by assuming that all collisions reaching the continuum eventually yield ions. At c.m. collision energies between 100 and 500 eV, we calculate that the total cross section for He*(2^3S) ionization ranges from 1×10^{-17} to 3×10^{-17} cm^2; it should be significantly larger for He*(2^1S) at these energies. At very high energies where almost 100% of the particles would be following the diabatic potential, the cross section becomes

$$\sigma_{ion} = \tfrac{1}{2} \pi R_x^2 ,$$

where the $\frac{1}{2}$ factor comes from the fact that only 50% of the He*(2^3S) + He particles follow the gerade potential curve, and R_x is the distance where the diabatic potential crosses into the $He_2^+ + e$ continuum. Since $R_x \approx 2.8a_0$, we obtain a high energy result for σ_{ion} of 3.4×10^{-16} cm^2, which is in extremely good agreement with the measurements of Gilbody *et al.*[31] in the c.m. energy range 15–175 keV.

To assess the contribution of collisional ionization to the destruction of fast metastable He in collisions with He target, we can compare these estimates of the ionization cross section with measured[32] total destruction cross sections σ_d. In the c.m. energy range 500–1100 eV, σ_d is $\sim 5 \times 10^{-16}$ cm^2 for He*(2^3S) and $\sim 8 \times 10^{-16}$ cm^2 for He*(2^1S), implying that ionization channels can account for a significant fraction of σ_d at keV energies.

Summary

We have discussed various mechanisms for collisional ionization in He* + He collisions and their relationship to the experimental He$^+$ distributions. Most of the structure can be understood in terms of a few ionization mechanisms involving an incoming repulsive diabatic potential. In the most prominent process the electron is ejected as the initial diabatic potential curve crosses into the continuum. Further ionization is found to occur near the distance of closest approach (as occurs in Penning ionization), and at crossings with higher continua. Contributions from Coulombic $He^+ + He^-$ states leading to long-range autoionization of He$^-$ are also possible. At high energies and small impact parameters, transitions to autoionizing neutral He** states are also expected. Even though most collisions occur along the $^{1,3}\Sigma_u^+$ or $^{1,3}\Sigma_g^+$ adiabatic potentials, the major contribution to ionization comes from those proceeding diabatically into the continuum. Significant contributions to ionization from the 2^1S metastable seem likely even though it is expected to be a minor component of the beam.

Note added in proof. A recent theoretical study by J. P. Gauyacq [J. Phys. B (to be published)] suggests the importance of $He^-(1s^2 2s) + He^+$ states in ground state He-He collisional ionization.

ACKNOWLEDGMENTS

We appreciate Dr. R. Morgenstern making available to use a preview of the electron energy distribution measurements from Freiburg. K.T.G. acknowledges helpful conversations with Dr. M. Barat, Dr. D. L. Huestis, Dr. D. C. Lorents, Dr. R. P. Saxon, and Dr. A. Salin regarding this work.

[†]This research was supported by the Office of Naval Research under Contract No. N00014-70-C-0339 and No. N00014-76-C-0118.

[1]K. T. Gillen, D. C. Lorents, R. E. Olson, and J. R. Peterson, J. Phys. B 7, L327 (1974).
[2]G. Gerber, R. Morgenstern, and A. Niehaus, J. Phys. B 6, 493 (1973).
[3]G. Gerber and A. Niehaus, J. Phys. B 9, 123 (1976).
[4]M. Barat, D. Dhuicq, R. Francois, C. Lesech, and R. McCarroll, J. Phys. B 6, 1206 (1973).
[5]J. C. Brenot, D. Dhuicq, J. P. Gauyacq, J. Pommier, V. Sidis, M. Barat, and E. Pollack, Phys. Rev. A 11, 1245 (1975).
[6]J. C. Brenot, D. Dhuicq, J. P. Gauyacq, J. Pommier, V. Sidis, M. Barat, and E. Pollack, Phys. Rev. A 11, 1933 (1975).
[7]F. J. Eriksen, S. M. Fernandez, A. B. Bray, and E. Pollack, Phys. Rev. A 11, 1239 (1975).

[8]R. Morgenstern, D. C. Lorents, J. R. Peterson, and R. E. Olson, Phys. Rev. A 8, 2372 (1973).
[9]R. E. Olson, E. J. Shipsey, and J. C. Browne (unpublished).
[10]G. H. Lantschner, thesis (Freiburg, 1975) (unpublished).
[11]M. L. Coleman, R. Hammond, and J. W. Dubrin, Chem. Phys. Lett. 19, 271 (1973).
[12]E. Holoien and J. Midtdal, Proc. Phys. Soc. A 68, 815 (1955).
[13]L. Lenamon, J. C. Browne, and R. E. Olson, Phys. Rev. A 8, 2380 (1973).
[14]S. A. Evans, J. S. Cohen, and N. F. Lane, Phys. Rev. A 4, 2235 (1971).
[15]R. P. Marchi and F. T. Smith, Phys. Rev. 139, A1025 (1965).
[16]B. Liu, Phys. Rev. Lett. 27, 1251 (1971).
[17]R. E. Olson, Phys. Rev. A 5, 2094 (1972).
[18]See also M. L. Ginter and R. Battino, J. Chem. Phys. 52, 4469 (1970); W. J. Steets and N. F. Lane, Phys. Rev. A 11, 1994 (1975); and Ref. 20.
[19]R. E. Olson and F. T. Smith, Phys. Rev. A 3, 1607 (1971).
[20]J. S. Cohen, Phys. Rev. A 13, 86 (1976).
[21]W. Lichten, Phys. Rev. 164, 131 (1967); M. Barat and W. Lichten, Phys. Rev. A 6, 211 (1972).
[22]S. L. Guberman and W. A. Goddard, III, Phys. Rev. A 12, 1203 (1975).
[23]R. P. Saxon, K. T. Gillen, and B. Liu, following paper, Phys. Rev. A 15, 543 (1977).
[24]W. H. Miller, J. Chem. Phys. 52, 3563 (1970).
[25]See, for example, review by M. Barat, *Invited Lectures and Progress Reports, Proceedings of the Eighth International Conference on the Physics of Atomic and Electronic Collisions* (Institute of Physics, Belgrade, 1973), p. 43.
[26]V. Sidis, J. Phys. B 6, 1188 (1973).
[27]M. Barat, D. Dhuicq, F. Francois, R. McCarroll, R. D. Piacentini, and A. Salin, J. Phys. B 5, 1343 (1972).
[28]G. J. Schulz, Rev. Mod. Phys. 45, 378 (1973).
[29]R. P. Madden and K. Codling, Astrophys. J. 141, 364 (1965).
[30]R. Morgenstern (private communication).
[31]H. B. Gilbody, K. F. Dunn, R. Browning, and C. J. Latimer, J. Phys. B 3, 1105 (1970).
[32]M. Hollstein, J. R. Sheridan, J. R. Peterson, and D. C. Lorents, Phys. Rev. A 187, 118 (1969).

Appendix B

THEORETICAL INVESTIGATION OF A MECHANISM FOR ION PRODUCTION IN COLLISIONS OF METASTABLE He WITH He: *Ab Initio* POTENTIAL CURVES FOR $^1\Sigma_g^+$ STATES OF He_2

PHYSICAL REVIEW A VOLUME 15, NUMBER 2 FEBRUARY 1977

Theoretical investigation of a mechanism for ion production in collisions of metastable He with He: *Ab initio* potential curves for $^1\Sigma_g{}^+$ states of He_2†

Roberta P. Saxon and Keith T. Gillen
Molecular Physics Center, Stanford Research Institute, Menlo Park, California 94025

Bowen Liu
IBM Research Laboratory, San Jose, California 95114

(Received 13 September 1976)

The mechanism of an observed ionization channel which produces He^+ at an energy loss of 18.7 ± 0.5 eV in 100–200-eV (c.m.) collisions of metastable He atoms with ground state He atoms was investigated. It is postulated that flux follows the diabatic singly excited $^1\Sigma_g{}^+$ state associated with $He^*(2\,^1S)$ projectiles and then transfers to the doubly excited $^1\Sigma_g{}^+$ state corresponding asymptotically to $2He^*(2\,^3S)$; autoionization follows at large internuclear separations. *Ab initio* calculations were performed on four He_2 states of $^1\Sigma_g{}^+$ symmetry for internuclear separations of $0.72a_0$ to $20.0a_0$. The classical deflection function for the mechanism stated above, generated from the calculated potentials, is consistent with the experimental angular distribution of the product ions.

INTRODUCTION

A large amount of physical insight into the details of atom-atom and ion-atom interactions has been gained in the last ten years from a combination of theoretical and experimental work on scattering processes involving light atoms or ions.[1] Much of the progress has been due to improvements in the computational techniques that have been used to generate the interaction potentials.

In the preceding paper, Gillen *et al.*[2] describe measurements of the ionization of a 100–400 eV metastable He* beam colliding with ground-state He

$$He^* + He \rightarrow He^+ + He + e^-. \tag{1}$$

One of the ionization features observed at center-of-mass (c.m.) collision energies $E_{cm} = 100$–200 eV (labeled feature D) yields He^+ ions at a c.m. translational energy loss of 18.7 ± 0.5 eV with an angular distribution peaking sharply at a value of $\tau = E_{cm}\theta_{cm} \approx 450 \pm 40$ eV deg. Although the metastable beam probably contains a much larger fraction of $He^*(2\,^3S)$ than $He^*(2\,^1S)$,[2] no mechanism involving the $2\,^3S$ component of the beam could be found to explain feature D. This paper postulates an ionization process involving the $2\,^1S$ projectiles as being responsible for this feature. We examine the requirements imposed by the experimental observations and verify, through *ab initio* calculations of interaction potentials and deflection function analysis, the ability of the proposed mechanism to match the experimental observations.

BACKGROUND

The most important properties of the experimental collisional ionization feature to be understood are the energy loss of 18.7 ± 0.5 eV and the sharp angular peaking at a reduced angle $\tau = E\theta$ of ~ 450 eV deg.

The constraint imposed by the small angle threshold for process D is the most stringent. In order to lose 18.7 eV of relative translational energy, the interacting particles must climb a steep repulsive wall which would give much larger deflection angles than those observed experimentally. To explain low angle scattering, one must invoke an inelastic transition to an excited curve which is strongly attractive at relatively small distances. This attraction would deflect the trajectories back to small scattering angles in a way similar to that previously described for the major ionization channel[3] (feature A) in this system.

As noted in the preceding paper,[2] energy loss values below 24 eV imply that the He^+ and He products are both in their ground electronic states and the excess energy loss above that necessary to ionize the metastable must reside in the outgoing electron energy. A fixed energy loss independent of scattering angle implies a fixed energy of the emitted electron. The postulated upper state with an inner well, required by low-angle scattering, must be a He_2 intermediate autoionizing state since the 18.7 eV energy loss does not allow any excited He_2^+ states to be populated. Autoionization of this intermediate state yields the ground state products and an electron whose kinetic energy is the difference between the measured energy loss and the energy loss necessary to ionize the metastable.

The fixed energy of the ejected electron independent of scattering angle requires that the observed ionization takes place at internuclear separations R where the potential curves for the upper auto-

ionizing molecular state and the final ion state are nearly parallel. This can most reasonably occur at large R where neither of the curves deviates significantly from its asymptotic limit. It also follows that the observed energy loss of 18.7 ± 0.5 eV is very nearly equal to the asymptotic energy difference between the initial state and the (intermediate) autoionizing molecular state.

The criterion of asymptotic energy difference may be used to determine the identity of the reactants and the products. The $He^*(2\,^3S) + He^*(2\,^3S)$ limit, the lowest limit with two excited He atoms, is asymptotically 19.0 eV higher than the $He^*(2\,^1S) + He(1\,^1S)$ limit and 19.8 eV higher than the $He^*(2\,^3S) + He(1\,^1S)$ limit. Therefore, the observed energy loss strongly suggests that the intermediate autoionizing state has the $He^*(2\,^3S) + He^*(2\,^3S)$ asymptote and that the initial reactant is the $2\,^1S$ component of the beam.

The identity of the molecular states involved may be determined by simple symmetry considerations. The two molecular states arising out of the $He^*(2\,^1S) + He(1\,^1S)$ asymptote have $^1\Sigma_g^+$ and $^1\Sigma_u^+$ symmetries, respectively, whereas the three states arising from the $He^*(2\,^3S) + He^*(2\,^3S)$ asymptote are of $^1\Sigma_g^+$, $^3\Sigma_u^+$, and $^5\Sigma_g^+$ symmetry, respectively. The only possible connection between these two sets of states is the radial coupling between the two $^1\Sigma_g^+$ states. It follows then that both the incoming and the outgoing molecular states are of the $^1\Sigma_g^+$ symmetry. In addition, earlier consideration of the observed small angular threshold already has led us to conclude that the upper $^1\Sigma_g^+$ states must have a deep potential well at small R.

Previous calculations[4,5] of the states of He_2 from the $2He^*(2\,^3S)$ asymptote, chiefly by Garrison *et al.*[5] only provided information at internuclear separations greater than $4a_0$. Their calculation for the $^1\Sigma_g^+$ state showed a well of ~0.6 eV depth near $6a_0$ and was repulsive at $4a_0$. However, the existence of a short-range well in the potential curve of the doubly excited $^1\Sigma_g^+$ diabatic state from the $2He^*(2\,^3S)$ asymptote is at least consistent with the following simple chemical consideration. At large R the 2s orbitals interact attractively and this is responsible for the long-range well. A barrier develops at smaller R due to electrostatic repulsion of the ion cores. At even smaller distances, however, there is strong bonding due to overlap of the core 1s orbitals and this may produce a deep inner well.

Therefore, all the experimental facts for ionization feature D might be consistent with the following mechanism. Analogously to the mechanisms found in the preceding paper, the reactants $He^*(2\,^1S) + He(1\,^1S)$ initially follow the repulsive diabatic $^1\Sigma_g^+$ potential curve into small internuclear separation. In this case, they can cross to the $^1\Sigma_g^+$ doubly excited curve in the region of a deep inner potential well and depart to large distances with ionization taking place where the $He^* + He^*$ curve is essentially parallel to the $He^* + He$ potential.

This model does not preclude ionization events at smaller R; these events would yield a distribution of energy losses and scattering angles that may be too diffuse to be observed in the laboratory. Ionization at the turning point (minimum R) might be very intense, but escape observation due to deflection to large angles where the intensity is masked by a large number of other ionization processes involving the $He^*(2\,^3S)$ or $He(1\,^1S)$ components of the beam. In contrast, all ionization events at large R values would yield nearly identical energy loss values (19 eV).

We have therefore undertaken multi-configuration self-consistent-field (MCSCF) calculations on four He_2 states of $^1\Sigma_g^+$ symmetry, the ground state, two singly excited states and the doubly excited state dissociating to two $He^*(2\,^3S)$ in order to look for the suggested well in the latter potential at small internuclear separations. The classical deflection function was then computed for the process in which the $He^*(2\,^1S)$ metastable initially follows the incoming singly excited diabatic potential and then follows the doubly excited autoionizing state on the outgoing channel. The classical deflection function was found to be in qualitative agreement with the experimental observation, lending support to this explanation of the 18.7 eV energy loss process.

METHOD OF CALCULATION

Approximations to the Born-Oppenheimer electronic wave functions and energies were calculated using the MCSCF method. The wave function of a desired electronic state was expanded in a limited N-particle basis set of orthonormal configuration state functions (CSF). Each CSF was a linear combination of Slater determinants (SD) such that it had the symmetry and multiplicity of the desired electronic state. The SD's were built from an orthonormal one-particle basis set of symmetry and equivalence restricted spatial orbitals. The spatial orbitals were expanded in terms of a basis set of Slater-type functions centered at the atomic nuclei. The expansion coefficients, both N- and one-particle, were determined variationally.

The He basis set used in our calculation is given in Table I. The 1s exponents are taken from the triple zeta basis of Clementi and Roetti.[6] The 2s

TABLE I. Orbital exponents.

1s	4.346	2p	4.17
1s	2.780	2p	2.09
1s	1.453	2p	1.04
2s	1.0	2p	0.52
2s	0.65		
2s	0.46		

exponents of Garrison *et al.*[5] from a double zeta set were augmented by an exponent of 1.0, the hydrogenic value for Be 2s and 2p, the united-atom limit of He_2. The largest 2p exponent was chosen to give a maximum overlap with the dominant 1s basis function, $\zeta = 2.780$. The remaining 2p exponents were taken to evenly span the space between 4.17 and approximately 0.5. The hydrogenic Be 2p value is included by the procedure.

The MCSCF calculations included all CSF's that can be constructed by distributing four electrons in four orbitals:

ground state: $1\sigma_g^2 1\sigma_u^2$,

singly excited: $1\sigma_g 1\sigma_u^2 2\sigma_g$

$1\sigma_g^2 1\sigma_u 2\sigma_u$,

doubly excited: $1\sigma_g^2 2\sigma_g^2$

$1\sigma_g^2 2\sigma_u^2$

$1\sigma_u^2 2\sigma_g^2$

$1\sigma_u^2 2\sigma_u^2$

$1\sigma_g 1\sigma_u(^1\Sigma_u^+) 2\sigma_g 2\sigma_u(^1\Sigma_u^+)$

$1\sigma_g 1\sigma_u(^3\Sigma_u^+) 2\sigma_g 2\sigma_u(^3\Sigma_u^+)$,

where the $1\sigma_g$ and $1\sigma_u$ orbitals correlate at the separated-atom limit, with the 1s orbitals of He, and $2\sigma_g$ and $2\sigma_u$ with the 2s orbitals. The wave functions for the four lowest $^1\Sigma_g^+$ states, within the manifold of the configurations listed above, were determined in a single MCSCF calculation where a weighted average of the energies of the four states was minimized. Since we were chiefly interested in the features of the doubly excited state, the highest state was weighted more heavily than the others in our calculations. To avoid numerical difficulties caused by linearly dependent basis functions at small internuclear separation, the overlap matrix was diagonalized and all eigenvectors with eigenvalues less than 1×10^{-5} were excluded from our calculations. The MCSCF program developed by J. Hinze was used in these calculations.

RESULTS AND DISCUSSION

Adiabatic potential curves for the singly and doubly excited $^1\Sigma_g^+$ states of He_2 are shown in Fig. 1, while data for all states calculated are given in Table II. The ionic curve to which the assumed autoionization occurs is also indicated. The diabatic potentials are indicated by the dashed lines. It is clear from the figure that the avoided crossing between the highest two adiabatic states (or actual crossing of the diabatic states) near $1.5a_0$ takes place over a rather narrow region. Exam-

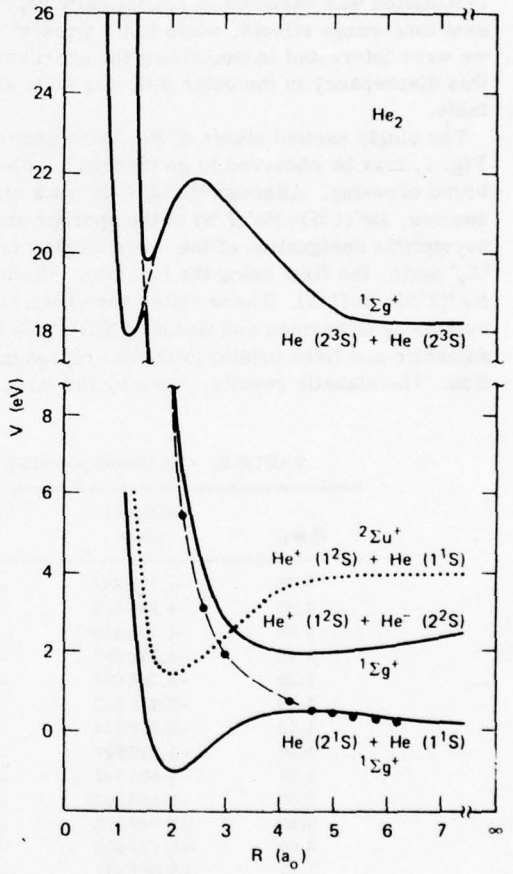

FIG. 1. Adiabatic He_2 $^1\Sigma_g^+$ potential curves calculated here are plotted with solid lines. Top curve is the doubly excited state. The other solid curves are singly excited states. The ground state has been omitted. Diabatic states are indicated by dashed lines. The points of Guberman and Goddard (Ref. 7), translated to agree asymptotically with the present calculation, are given by large dots. The dotted curve approximates the $^2\Sigma_u^+$ state of He_2^+. Although $He^-(2\,^2S)$ is not a stable species, $He^+(1\,^2S) + He^-(2\,^2S)$ is the appropriate asymptotic designation of the higher singly excited state. Asymptotically it lies above the $^2\Sigma_u^+$ He_2^+ state.

ination of the coefficients of the CSF's in the wave functions shows that the crossing occurs between $1.4a_0$ and $2.0a_0$. Thus the description of the diabatic potential by simply drawing a smooth curve connecting points in the adiabatic noncrossing region was quite reasonable for our purposes here.

The doubly excited diabatic potential curve showed the expected inner attractive well at about $1.4a_0$. It is bound by approximately 0.4 eV with respect to the two $He^*(2\,^3S)$ asymptote and is approximately 4.0 eV lower than the hump in the potential curve at $2.5a_0$. The potential also is attractive at long range, in this calculation being bound by about 0.13 eV around $7a_0$. The calculation of Garrison *et al.*[5] gave a depth for the outer well at 0.56 eV at an R_e of $6.34a_0$. Since their calculation was designed to realistically represent long-range effects, while in the present work we were interested in describing the short range, this discrepancy in the outer well was quite acceptable.

The singly excited states of He_2, also shown in Fig. 1, may be observed to go through a rather broad crossing. Although $He^-(2\,^2S)$ is not a stable species, $He^*(1\,^2S) + He^-(2\,^2S)$ is the appropriate asymptotic designation of the other singly excited $^1\Sigma_g^+$ state, the first being the incoming channel, $He^*(2\,^1S) + He(1\,^1S)$. These states have been calculated by Guberman and Goddard (GG)[7] both in an adiabatic and fixed orbital (diabatic) representation. The diabatic results, given by the large dots in Fig. 1 smoothly connect the adiabatic potentials calculated here. The points have been translated upward by 0.05062 a.u. to bring the asymptote into agreement with the present calculation. Their adiabatic calculation had a well depth with respect to the asymptote of 0.644 eV at $R_e = 2.17a_0$ compared with 1.18 eV at $R_e = 2.13a_0$ for the present work. The singly and doubly excited He_2 $^1\Sigma_g^+$ states also have been included in a calculation by Gauyacq,[8] but the incoming diabatic state appropriate to this experiment has not been estimated in that work. A calculation[9] of the ground state and lowest doubly excited state of He_2 at very small internuclear distances produced a higher energy at $2.0a_0$ than at $1.0a_0$ for the upper adiabatic state, but the implication of a possible well at intermediate distances was not discussed. Another recent calculation[10] using a very simplified model gave a diabatic doubly excited $^1\Sigma_g^+$ state in qualitative agreement with the present results.

The classical deflection function for a curve-crossing collision was calculated using the procedures outlined by Olson and Smith.[11] In this calculation the initial state was assumed to be the diabatic $^1\Sigma_g^+$ state correlating asymptotically to $He^*(2\,^1S) + He(1\,^1S)$ since the state correlating adiabatically to the reactants cannot interact with the outgoing molecular state except at very small R (Table II) and must therefore yield unacceptably large deflection angles. The outgoing state in the deflection function calculation was the autoionizing

TABLE II. Calculated potential curves for four $^1\Sigma_g^+$ states of He_2 in atomic units.

R (a_0)	Ground state	Singly excited states		Doubly excited states
0.75	−4.105 283	−4.027 943	−3.970 071	−2.177 459
0.80	−4.263 832	−4.177 596	−4.073 123	−2.442 453
1.00	−4.735 469	−4.579 067	−4.275 862	−3.241 114
1.15	−4.978 981	−4.754 282	−4.313 941	−3.653 895
1.25	−5.106 667	−4.833 966	−4.314 419	−3.868 054
1.35	−5.212 513	−4.892 529	−4.304 558	−4.044 137
1.40	−5.258 314	−4.915 601	−4.297 587	−4.119 744
1.50	−5.337 807	−4.951 567	−4.290 011	−4.241 862
1.75	−5.480 107	−4.999 543	−4.498 044	−4.226 374
2.00	−5.566 201	−5.012 056	−4.649 280	−4.189 862
2.50	−5.648 266	−4.996 064	−4.807 032	−4.167 825
3.00	−5.677 560	−4.972 506	−4.869 955	−4.187 746
3.50	−5.687 938	−4.959 292	−4.891 901	−4.217 097
4.00	−5.691 368	−4.953 899	−4.898 389	−4.245 627
4.50	−5.692 148	−4.952 413	−4.899 824	−4.269 326
5.00	−5.691 904	−4.953 612	−4.898 843	−4.285 788
6.00	−5.690 849	−4.958 575	−4.893 131	−4.300 947
7.00	−5.690 111	−4.962 788	−4.885 073	−4.303 330
8.00	−5.689.939	−4.966 215	−4.874 653	−4.302 298
10.00	−5.690 146	−4.969 825	−4.855 172	−4.300 442
20.00	−5.690 028	−4.970 835	−4.812 138	−4.298 498

state correlating to $2He^*(2^3S)$. To obtain the diabatic potential for the incoming channel, the following points were smoothly connected: values from the highest adiabatic state for $0.75a_0 < R < 1.4a_0$, the second to highest for $1.5a_0 < R < 2a_0$, GG values at 2.6, 3.0 and 4.2 a_0, and values for the third adiabatic state for $R > 4.5a_0$, where the crossing was bridged as shown by the dashed line. The *ab initio* calculation gave the asymptotic separation of the incoming and outgoing states as 18.295 eV. For the deflection function calculation, the upper curve was translated to the spectroscopic separation of 19.023 eV.

The branch of the deflection function that yields the minimum scattering angle at each impact parameter is the one for which the particle goes adiabatically in its first transit of the crossing at $R \sim 1.5a_0$ and diabatically in its second transit. That branch of the deflection function for a collision energy of 100 eV is plotted vs impact parameter in Fig. 2. The smallest scattering angle found in the deflection function is approximately 3.0° (300 eV deg).

From this minimum in the deflection function, the semiclassical Airy function analysis of Ford and Wheeler[12] was used to predict a quantum mechanical rainbow at $\tau \approx 490$ eV deg. The experimental cross section peaks sharply at 450 eV deg and is in excellent agreement. At wider scattering angles, other processes not considered in this paper also contribute to the 19-eV loss,[2] but the isolated feature peaking at small angles and an energy loss of 18.7 eV is certainly totally consistent with the assumed mechanism.

It may be noted that the calculation of Garrison *et al.*,[5] which is expected to be the most reliable at large internuclear separations, had an outer well approximately 0.56 eV deep. If molecular ionization takes place in this outer well region rather than at larger distances, the energy loss could be lower than the asymptotic 19.0 eV value by the amount of the well depth. The measured energy loss of 18.7 ± 0.5 eV allows this possibility, and the deflection function for this process would deviate insignificantly from the case where ionization occurs at larger distances.

Long-range molecular autoionization from the same doubly excited state discussed here has, however, also been observed by Gerber *et al.*[13] in the case of ground state He + He collisions. The electron energy distribution[14] for autoionization from this same $^1\Sigma_g^+$ excited state peaks at 15.0 eV at a collision energy comparable to ours; this would imply an energy loss peaking at 19.0 eV in our experiment.

The present experimental data by no means precludes the existence of intense ionization at the turning point since that process would yield scattering at wide angles which would be difficult to resolve from other channels; but the evidence of long-range autoionization cannot be taken lightly as it suggests that an observable fraction of the doubly excited reactants escape from small R without having autoionized. This result also predicts the observation of scattered neutral $He^*(2^3S) + He^*(2^3S)$ products with the same angular distribution and energy loss as that of the observed He^+ ions since autoionization at large R also undoubtedly takes place with less than unit probability. A similar prediction for ground-state He + He collisions has been confirmed by Morgenstern *et al.*[15] and studied in detail by Brenot *et al.*[16]

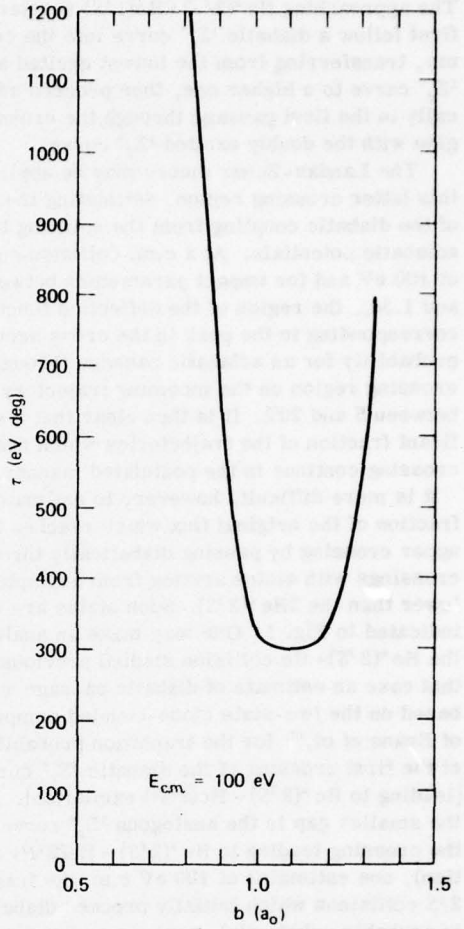

FIG. 2. Reduced classical deflection function $\tau = E_{cm}\theta$ (where θ is the c.m. deflection angle) plotted versus impact parameter b for a collision where the initial channel is the diabatic state correlating to $He^*(2^1S) + He(1^1S)$, the final channel is the diabatic state correlating to $2He^*(2^3S)$, and the flux transfers from the initial to the final channel the first time it traverses the crossing.

Finally, it is desirable to estimate the probability for following the postulated potential curves. The approaching $He^*(2^1S) + He(1^1S)$ reactants must first follow a diabatic $^1\Sigma_g^+$ curve into the continuum, transferring from the lowest excited adiabatic $^1\Sigma_g^+$ curve to a higher one, then proceed adiabatically in the first passage through the crossing region with the doubly excited $^1\Sigma_g^+$ curve.

The Landau-Zener theory may be applied in this latter crossing region, estimating the strength of the diabatic coupling from the splitting between adiabatic potentials. At a c.m. collision energy of 100 eV and for impact parameters between $0.9a_0$ and $1.3a_0$, the region of the deflection function corresponding to the peak in the cross section, the probability for an adiabatic passage through this crossing region on the incoming trajectory lies between 5 and 20%. It is then clear that a significant fraction of the trajectories which reach this crossing continue in the postulated manner.

It is more difficult, however, to estimate the fraction of the original flux which reaches this upper crossing by passing diabatically through crossings with states arising from asymptotes lower than the $2He^*(2^3S)$. Such states are not indicated in Fig. 1. One may make an analogy to the $He^*(2^3S) + He$ collision studied previously.[3] In that case an estimate of diabatic passage was based on the two-state close-coupled computations of Evans *et al.*[17] for the transition probabilities at the first crossing of the diabatic $^3\Sigma_g^+$ curve [leading to $He^*(2^3S) - He(2^3P)$ excitation]. From the smaller gap in the analogous $^1\Sigma_g^+$ curves[7] (at the crossing leading to $He^*(2^1S) - He(2^1P)$ excitation), one estimates at 100 eV c.m. the fraction of 2^1S collisions which initially proceed diabatically is probably substantial, perhaps as much as 30–40% of those following the incoming $^1\Sigma_g^+$ potential. In estimating the probability of diabatic passage through subsequent crossings, it may be assumed that coupling matrix elements for the singlet manifold are similar to those for the triplet states, which have been calculated by Cohen.[18] From these triplet matrix elements, the Landau-Zener theory predicts a probability of 80% for going diabatically through all subsequent crossings for the impact parameters considered here.

The above result has interesting implications for the energy dependence of feature D. At higher collision energies than 100 eV, a smaller probability of adiabatic passage through the final crossing with the outgoing $2He^*(2^3S)$ state would tend to decrease the cross section. This fraction might be compensated somewhat by an increase with energy in the fraction proceeding diabatically into the continuum, although that fraction is already quite large at 100 eV. Since the total ionization cross sections for both the singlet and triplet metastables are expected to increase substantially with energy as the initial diabatic probability increases, the fractional contribution from process D to the total cross section may be expected to decrease as the relative energy increases beyond 100 eV.

No direct experimental comparison of the intensity of feature D with the other ionization channels can be made, since the ratio of $He^*(2^1S)$ to $He^*(2^3S)$ in the beam is unknown and may even vary considerably with beam energy. Nevertheless, the expected energy dependence leads to the conclusion that this channel might be more difficult to observe at collision energies higher than those studied here. This is especially true in measurements of the emitted electron energy, where electrons produced at the turning point (process B^2) yield an intense continuum electron energy distribution. Any attempt to measure the 15 eV electrons from process D through the interfering continuum should emphasize procedures that minimize the relative contribution from other ionization channels, e.g., by working at low collision energies and by attempting to maximize the beam fraction of $He^*(2^1S)$.

In summary, the calculations reported here were undertaken to investigate the mechanism of He^+ ion production at an energy loss of 18.7 eV in collisions of metastable He atoms with ground-state He atoms. The results are consistent with the postulated ionization mechanism that flux follows the diabatic singly excited $^1\Sigma_g^+$ state associated with $He^*(2^1S)$ projectiles and then transfers to the doubly excited $^1\Sigma_g^+$ state corresponding asymptotically to $2He^*(2^3S)$. It also appears that molecular autoionization occurs from the latter state at large internuclear separations where it is essentially parallel to the He_2^+ potential.

Note added in proof. It has come to our attention that some of the states calculated here also have been determined by J. P. Gauyacq [J. Phys. B (to be published)] in his study of ion production in He ground-state, ground-state collisions.

ACKNOWLEDGMENT

We gratefully acknowledge the usual enlightening conversations with Dr. R. E. Olson.

†R.P.S. supported by Atmospheric Sciences Section, National Science Foundation Grant ATM-74-23738; K.T.G. supported by Office of Naval Research.

[1]See for example: M. Barat, Invited Lectures and Progress Reports, *Seventh International Conference on Electronic and Atomic Collisions, Beograd, 1973* (North-Holland, Amsterdam, 1971), p. 43; R. McCarroll, *ibid.*, p. 71.

[2]K. T. Gillen, J. R. Peterson, and R. E. Olson, preceding paper, Phys. Rev. A 15, 527 (1977).

[3]K. T. Gillen, D. C. Lorents, R. E. Olson, and J. R. Peterson, J. Phys. B 7, L327 (1974).

[4]D. J. Klein, J. Chem. Phys. 50, 5151 (1969).

[5]B. J. Garrison, W. H. Miller, and H. F. Schaefer, J. Chem. Phys. 59, 3193 (1973).

[6]E. Clementi and C. Roetti, At. Data Nucl. Data Tables 14, 177 (1974).

[7]S. L. Guberman and W. A. Goddard, III, Chem. Phys. Lett. 14, 460 (1972); Phys. Rev. A 12, 1203 (1975); S. Guberman, thesis (Cal Tech, 1972) (unpublished).

[8]J. P. Gauyacq, J. Phys. B 9, 2289 (1976).

[9]D. R. Yarkony and H. F. Schaefer, III, J. Chem. Phys. 61, 4921 (1974).

[10]T. M. Kereselidze Zh. Eksp. Teor. Fiz. 69, 67 (1975) [Sov. Phys.-JETP 42, 33 (1976)].

[11]R. E. Olson and F. T. Smith, Phys. Rev A 3, 1607 (1971).

[12]K. W. Ford and J. A. Wheeler, Ann. Phys. (N.Y.) 1, 259 (1959).

[13]G. Gerber, R. Morgenstern, and A. Niehaus, J. Phys. B 6, 493 (1973); see also M. Barat, D. Dhuicq, R. Francois, C. Lesech, and R. McCarroll, J. Phys. B 6, 1206 (1973).

[14]G. Gerber and A. Niehaus, J. Phys. B 9, 123 (1976).

[15]R. Morgenstern, M. Barat, and D. C. Lorents, J. Phys. B 6, L330 (1973).

[16]J. C. Brenot, D. Dhuicq, J. P. Gauyacq, J. Pommier, V. Sidis, M. xxx at, and E. Pollack, Phys. Rev. A 11, 1245 (1975).

[17]S. A. Evans, J. S. Cohen, and N. F. Lane, Phys. Rev. A 4, 2235 (1971).

[18]J. S. Cohen, Phys. Rev. A 13, 86 (1976).

Appendix C

METASTABLE RARE GAS COLLISIONS AT INTERMEDIATE ENERGIES (5-3000 eV)

METASTABLE RARE GAS COLLISIONS AT INTERMEDIATE ENERGIES (5-3000 eV)*

Keith T. Gillen
Molecular Physics Center
SRI International (Stanford Research Institute)
Menlo Park, California 94025 U.S.A.

INTRODUCTION

Appreciation of the detailed dynamical information available from scattering experiments has caused a tremendous increase in the quantity and quality of collisional work in the two decades since the first ICPEAC. However, it is only in the last few years that experimental work involving electronically excited projectiles has made a significant contribution to our understanding of collisional processes. For several reasons much of this work has involved metastable rare gases. Metastable rare gas beams can be efficiently produced at thermal energies by electron bombardment of neutral atoms and at higher energies (> 10 eV) by near-resonant charge transfer of rare gas ions; efficient detectors exist for single particle counting techniques. The metastable electronic energy levels for the rare gases vary over a wide range (8.3 eV - 20.6 eV), allowing a myriad of processes to be studied in a systematic manner. Finally, there exists intense interest in visible and uv laser systems involving various modes of transfer of electronic excitation from metastable rare gas atoms and dimers to other species.[1] Hence, metastable rare gas interactions are now and should remain important prototype systems for the understanding of many of the general properties of excited state interactions.

Experiments near thermal energies[2] are generally more directly relevant to the understanding of discharges, lasers, and other excited media, and often have the advantage over experiments at higher energies that only a few potential energy surfaces are energetically accessible. However, despite the added complications and less direct relevance of experiments at moderate energies (> 5 eV), they have unique advantages as well.

Firstly, thermal energy experiments will not always be able to explore important regions of the interaction potentials at small internuclear distance r. That fact is obvious for consideration of important couplings between potential surfaces high on their inner repulsive walls. Less obvious is the problem

associated with the investigation of deep chemical (excimer) wells. Thermal collisions which are very sensitive to shallow outer (van der Waals) wells may not have sufficient energy to surmount the small barrier between the van der Waals well and the deep inner well. Even if the inner well region is explored,[3] the resultant scattering may be too diffuse to yield any details on the shape of the potential. Interactions at moderate energies, in contrast, are not sensitive to shallow van der Waal's wells and small barriers; hence one can concentrate on potential surface features at distances inside the van der Waal's region. Recent work of Trujillo[4] on velocity selected beams of metastable He from an arc heated source spans the beam energy range from thermal to 10 eV. This technique also holds considerable promise for studies of deep chemical wells.

Secondly, the easy variation of collision energy possible with charge transfer production techniques allows observed collisional features to be examined over a large energy range. This fact can often help to unravel complicated scattering patterns associated with the large number of potential surfaces accessible in a collision system; characteristics of the energy dependence associated with a given feature can often be used to infer the mechanism involved. Hence by spanning a range of collision energy, one can hope to observe, characterize, and identify at least the major collisional features important in different energy regimes.

A third advantage for studying metastable interactions at elevated energies is the existence of a large body of detailed work on electronic excitation in collisions of ground state ions and atoms with various targets in this same energy range. This work[5] not only has led to a characterization of the energy and angular dependence of the scattering associated with various prototype surface coupling mechanisms, but also has yielded results directly applicable to the metastable interaction experiments. For example, the He^* + He collision, which I plan to discuss at length in this report, explores the same set of potential surfaces applicable to He + He collisions and its core (1s electron) interaction might be expected to have many similarities to the well-studied He^+ + He system. Since intermediate energy metastable scattering has not been reviewed previously, I will briefly summarize the experimental accomplishments in this area in addition to a more detailed discussion of very recent work on the He^* + He system. Recent progress on elastic scattering of metastable rare gases at lower energies is being reviewed elsewhere in this book.[6]

EXPERIMENTAL

Near-resonant charge transfer of rare gas ion beams in alkali targets[7] can efficiently produce metastable rare gas beams of energies greater than 10 eV. The beam produced can then be caused to interact with another beam or with a target gas; and the product ions, electrons, photons, or neutral atoms can be detected.

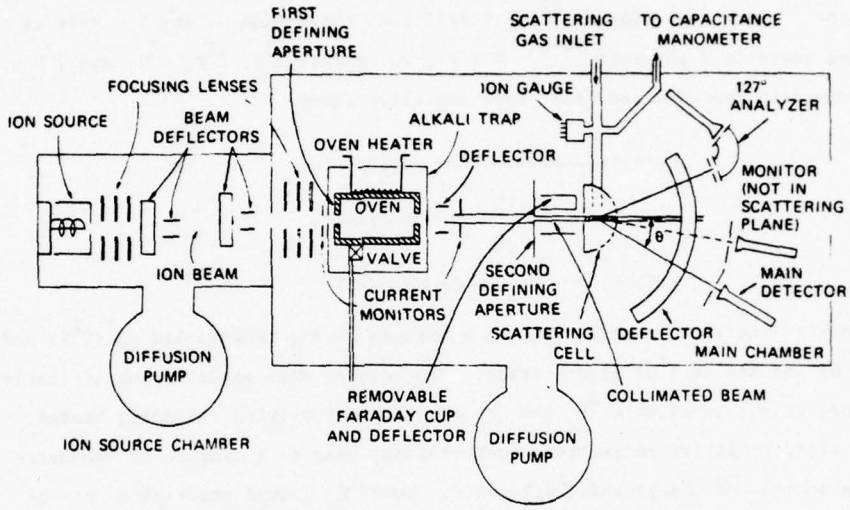

Fig. 1. Metastable Differential Scattering Apparatus at SRI

Shown in Figure 1 is a differential scattering apparatus[8] at SRI where both product ions and neutrals can be examined. Rare gas ions are extracted from a discharge and focussed into a charge transfer cell filled with alkali vapor. The product fast neutral beam (after deflection of unreacted parent ions) enters a collision cell filled with target gas. Rotating around this cell are two channeltron detectors. One channeltron is mounted behind an energy analyzer and can measure the energy and angular distribution of product ions. The other detector views the scattering cell directly and is generally used to measure the angular distribution of product neutrals, whose energy spectrum can be determined by a time-of-flight (tof) technique involving electrical pulsing of the parent ion beam before it enters the charge transfer cell.

Clearly, this apparatus uses a slight modification of techniques commonly applied to ion-atom scattering. Other experimental techniques applied so far in this energy range (5 eV to 3 KeV) are also similar alterations of ion atom

experiments. Hence, I will concentrate here on a couple of experimental problems unique to metastable collision studies.

Charge Transfer and Beam Composition

For each rare gas ion R^+, one or more alkali atoms M can be found where charge transfer into the lowest excited rare gas neutral states

$$R^+ + M \rightarrow R^* + M^+$$

is nearly resonant. At beam energies above approximately 10 eV, these cross sections[7,9] are large (10-100 $\AA^2$) and efficient conversion of the ion beam to excited neutrals is possible.[10-12] For He, the states 2^1S, 2^1P, 2^3S, and 2^3P are predominantly produced and after fast radiative decay

$$He(2^1P) \xrightarrow{99.9\%} He(1^1S)$$
$$\qquad\quad \xrightarrow{0.1\%} He^*(2^1S)$$

and

$$He(2^3P) \longrightarrow He^*(2^3S) \quad ,$$

the forward scattered neutral beam is a mixture of the metastables $He^*(2^1S)$ and $He^*(2^3S)$ and the $He(1^1S)$ ground state. The heavier rare gases can be similarly produced in the metastable $^3P_2$ and $^3P_0$ levels and low-lying radiating states. Again after radiative relaxation, the resultant beam is a mixture of two metastable states and the ground ($^1S_0$) state. Some $^1S_0$ ground state atoms may be formed directly in the charge transfer step by production of alkali ions in excited electronic states.[13]

Although these charge transfer techniques have been used widely to produce metastable beams of energy greater than 10 eV there exists no complete experimental determination of the composition of any beam produced in this way. Several theoretical investigations of the charge transfer reaction have yielded estimates of the composition of the neutral beams,[10-12] but the calculations are of unknown reliability and have not been adequately tested against experimental measurements. For He^+ charge transfer with Cs, theoretical calculations predict a large ratio of $He^*(2^3S)$ to $He^*(2^1S)$ in the beam.[10,11a] Experimental evidence for this same conclusion exists at beam energies below 50 eV from rainbow scattering experiments on $He^* + He$[8] and from $He^*(2^1S)$ removal by a quench lamp technique.[14] Neither experiment, however, yielded information on the fraction of $He(1^1S)$ in the beam. Recently Neynaber and Magnusen[15] in a merged beam experiment determined the $He(1^1S)$ fraction by monitoring its subsequent reactions with various ions under

conditions where reaction of the metastable components would be unobservable. Their results for several charge transfer pairs at energies above 1 KeV gave no information on the relative populations of the two metastable components. [The first complete determinations of state populations for fast, charge-transfer produced He beams were reported at the Paris ICPEAC, see Ref. 63.]

When using a mixed beam of unknown composition for subsequent scattering experiments, one must obviously be careful that a specific scattering feature is identified with the beam component responsible. The effects of the ground state are easiest to surmise, since one can produce and scatter a pure ground state rare gas neutral beam of the same energy by replacing the near-resonant alkali charge transfer step with a resonant charge transfer in the parent rare gas.

Separating the contributions from the two metastable states is not as simple. Often a knowledge of the relevant interaction potentials[8,16] or a clever choice of experimental conditions[17] will allow one to associate a specific scattering feature with one of the metastable states in the beam. Otherwise a certain ambiguity remains.

At thermal energies a quench lamp can be used to remove the 2^1S component from a He^* beam[18a]

$$He^*(2^1S) + h\nu(2.06\mu) \longrightarrow He(2^1P) \xrightarrow[584\text{Å}]{h\nu} He(1^1S) \quad ,$$

allowing separate determinations of $He^*(2^1S)$ and $He^*(2^3S)$ scattering. At energies above a few tens of eV, the absorption line is Doppler shifted far enough out of resonance that the quench lamp cannot efficiently[14] depopulate the $He^*(2^1S)$. The problems caused by the Doppler shift for moderate energy beams imply that either intense tunable or broad band light sources should be more successful quenchers, and laser-induced-fluorescence techniques could eventually be used to monitor and alter beam compositions.[18b]

Detection Efficiencies

Scattered particles are detected individually on channeltrons and the key determinant of the detection efficiency is the secondary electron ejection coefficient for the particle on the surface of the channeltron. Electrons or ions can be pulled into the detector at high energy and detected with efficiency near unity;[19] however, neutral particle energies cannot be altered as they enter the detector. Little is known about the secondary electron ejection efficiency

of metastables at moderate energies,[20] although the detection efficiency ratios[8,21] of He^+ to $He(1^1S)$ and $He^*(2^3S)$ have been determined. Operating at high enough energies that the detection efficiency is comparable for R^+, R, and R^* is the best way to remove any ambiguities caused by variations in detection efficiencies. For He this energy is approximately 400 eV. On the contrary, one often prefers to have large differences in detection efficiency. To observe g-u symmetry oscillations[22,23] from excitation exchange channels

$$R^* + R \rightarrow R + R^* \quad ,$$

one must choose energies where the detection efficiencies for R^* and R differ significantly. At low energies, ground state rare gas atoms have very low detection efficiencies and pure metastable scattering[6,8,16] can be studied.

RESULTS

A compilation of experimental results for moderate energy (5-3000 eV) collisions involving rare gas metastable atoms is presented[65] in Table 1. Several aspects of the tabulation need be explained. First, a specific metastable beam state is indicated when experimental evidence exists to indicate that the observed scattering can be associated with that particular component of the beam. When both states are specified in He^* total destruction cross section experiments, the two attenuation cross sections have been determined separately by a technique that monitors the decrease in each metastable component.[17] The merged beam technique is capable of total cross section measurements and limited differential scattering information spanning the c.m. energy range from thermal to the kilovolt region; however, only those systems which have been studied at energies above 5 eV are listed here. Worth special note is the merged beam measurement of associative ionization involving two metastables He^* and Ne^*. Preliminary total cross section measurements[4] of Trujillo on He^* scattering that extend from thermal energies to just above the lower limit of the energy range tabulated here have also been omitted, but should be noted (see also Ref. 64).

It is clear from Table 1 that the experiments so far have only examined a small fraction of the potentially interesting collision systems involving rare gas metastables in this energy regime. Optical data are negligible. There exist almost no inelastic data in the keV energy range where so much work on ground state neutral and ion scattering exists. Rearrangement ionization has hardly been explored; no other chemical reactions have been examined, even though

TABLE 1: Metastable Rare Gas Scattering (5-3000 eV c.m.)

Projectile	Target	Measurement	Energy Range (c.m.)	Ref.
He^*	H,D	MB	0.05-10 eV	24
He^*	H_2	Op	370	25
He^*	H_2	RI	0.05-10	26
He^*	He	AT	300	27
$He^*(2^3S)$	He	TD	11-86	28
$He^*(2^3S,2^1S)$	He	TD	75-1100	17
He^*	He	Op	550	25
$He^*(2^3S)$	He	A	5-10	8
$He^*(2^3S)$	He	TOF	8.6	29
He^*	He	E,TOF,(I)	600-2500,500-700	30
He^*	He	I	50-200	31-33
He^*	Ne	Op	920	25
He^*	Ne^*	MB	0.01-10	34
He^*	C_2H_2	TD	60-520	35
$He^*(2^3S,2^1S)$	N_2	TD	40-1300	35
He^*	N_2	Op	960	25
$He^*(2^3S,2^1S)$	Ar	TD	64-1360	35
He^*	Ar	E	9-91	36
He^*	Ar	A	360-1800	37
He^*	Xe	E	8-97	36
He^*	Xe	E	29-485	38
Ne^*	H_2,HD,D_2	RI	2.5-17	39
$Ne^*(^3P_2)$	Ne	A	7-53	23
Ne^*	Ar	TD	80-400	35
Ne^*	Ar	MB	0.01-600	40
Ne^*	Kr	MB	0.01-10	41
Ne^*	Xe	E	13-87	36
Ar^*	C_2H_2	TD	40-240	35
$Ar^*(^3P_2)$	Ar	A	5-75	16,22

Measurements

- AT Attenuation total cross sections
- TD Total metastable destruction cross sections (attenuation techniques)
- MB Merged beam Penning and Associative Ionization Cross Sections
- Op Optical relative cross sections for line emission
- E Product electron energy distributions
- A Angular distribution measurements
- TOF Time-of-flight inelastic scattering
- I Product ion energy-angle distributions
- RI Rearrangement ionization, $R^* + H_2 \rightarrow RH^+ + H + e^-$

metastable rare gases have properties that suggest strong analogies to the very well studied[42] reactions of alkali atoms. Inelastic differential cross section data is of low resolution and has only been applied to the He^* + He system. High resolution data are available for product electron energy distributions, but have only been published for the collision systems He^* + He and He^* + Xe.

The system that has received the most experimental (and theoretical) attention so far is He^* + He. In the next section I will examine this collision pair in more detail and try to summarize the most important inelastic channels observed. This system, although far from completely characterized, can still serve as a model for indicating the amount of experimental detail possible with the presently available experimental tools. In the next few years, techniques for determining and modifying metastable beam populations[18] should improve considerably, and many more systems will have been studied in much greater detail than He^* + He has been today.

He^* + He Inelastic Scattering

For ground state He-He collisions, experimental work measuring differential inelastic scattering,[21,43,44] product electron energy distributions,[45,46] and optical emissions[47,48] from collisionally excited states has produced a reasonable understanding of the major excitation processes involved. A useful way in which to introduce the framework for discussion of He^* + He collisions is to consider first the important inelastic mechanisms found for ground state interactions.

The simplest starting point for a consideration of the He_2 collision system is the schematic molecular orbital (MO) correlation diagram[49] shown in Figure 2. Only the important, low-lying molecular orbitals are shown. Using nomenclature appropriate to the united atom limit, the incoming $^1\Sigma_g^+$ state for He-He collisions is designated $1s\sigma_g^2 2p\sigma_u^2$. As the two He atoms approach each other, the only obvious inelastic transitions involve a two-electron $2p\sigma_u^2 \rightarrow 2s\sigma_g^2$ potential coupling (radial coupling in an adiabatic description) at $\sim 0.6\ a_o$ and one and two electron rotational couplings in the united atom limit between the $2p\sigma_u$ and $2p\pi_u$ orbitals. Consideration of a molecular state correlation diagram derived from the set of possible orbital occupancies shows that $2p\sigma_u^2 \rightarrow 2s\sigma_g 3s\sigma_g$ is also possible at small distance, since the united atom $Be(1s^2 2s3s)\ ^1S$ state lies below the $Be(1s^2 2p^2)\ ^1P, ^1S$ levels. However, this transition would not be expected to be important except for very violent collisions.[50] The important primary transitions along the entrance channel are

$$1s\sigma_g^2 2p\sigma_u^2(^1\Sigma_g^+) \rightarrow 1s\sigma_g^2 2s\sigma_g^2(^1\Sigma_g^+) \qquad \text{I}$$

$$1s\sigma_g^2 2p\sigma_u^2(^1\Sigma_g^+) \rightarrow 1s\sigma_g^2 2p\sigma_u 2p\pi_u(^1\Pi_g) \qquad \text{II}$$

$$1s\sigma_g^2 2p\sigma_u^2(^1\Sigma_g^+) \rightarrow 1s\sigma_g^2 2p\pi_u^2(^1\Delta_g \text{ and } ^1\Sigma_g^+) \quad . \qquad \text{III}$$

Excitation III involves a two electron transition, with the $^1\Delta_g$ state produced by a two-step rotational coupling and the $^1\Sigma_g^+$ state produced either by a two-step rotational transition through the $^1\Pi_g$ state or by direct potential coupling.

As the atoms separate, the primary excitations would in the simplest picture produce

$$\text{I} \rightarrow 2\text{He}(1s2s)\,^3S$$

$$\text{II} \rightarrow \text{He} + \text{He}(1s2p)\,^1P$$

$$\text{III} \rightarrow 2\text{He}(1s2p) \quad .$$

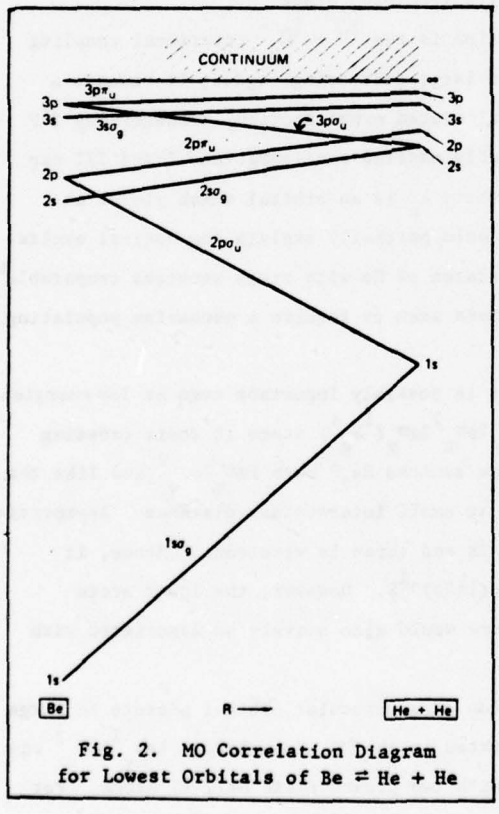

Fig. 2. MO Correlation Diagram for Lowest Orbitals of Be ⇌ He + He

The experimental and theoretical[50-52] results for He-He collisions indicate that primary excitations II and I are respectively the most important one and two electron excitation processes for low collision energies (below ~ 200 eV c.m.). High resolution inelastic[44] tof data shows the importance of these two product channels; and the theoretical calculations agree well with the shapes and magnitudes of the differential cross section. Optical measurements[47] show a dominant $He(2^1P)$ emission. Structure in the electron energy distribution is dominated[45,46] by a peak at 15 eV which is caused by long range autoionization along the $^1\Sigma_g^+$ state (produced in I) when it is nearly parallel to (and the asymptotic 15 eV above) the lowest He_2^+

potential. Theoretical calculations by Olson et al.[51] verify that the rotational coupling between the $1s\sigma_g^2 2p\sigma_u 2p\pi_u(^1\Pi_g)$ and the $1s\sigma_g^2 2p\sigma_u 3p\sigma_u(^1\Sigma_g^+)$ configurations at large r ($\sim 4\ a_o$) does not produce more than a 10% transfer of 2^1P excitation to the 2^1S state.

At higher energies primary coupling III begins to dominate contributions to the double excitation process as the potential coupling associated with I decreases in importance. Inelastic tof profiles for two electron excitations[44] are dominated by a peak with an energy loss value corresponding to excitation of two $He(2^1P)$ atoms. Electron energy distributions[46] show the emergence of a feature at an energy corresponding to molecular autoionization at large distances on that same potential. However, both the tof and the electron measurements clearly show the importance of other states not purely associated with the primary coupling mechanisms; and optical measurements[48] show the importance of n = 3 and n = 4 excitations. These additional states must be produced by secondary interactions transferring excitation from configurations I-III to other configurations that are crossed as the excited atoms separate from each other.

An example of a secondary interaction is the $^1\Pi \rightarrow {}^1\Sigma_g^+$ rotational coupling considered above. At high energies and large scattering angles, it becomes a more important contribution[50] to the calculated cross section, transferring 2^1P excitation into the 2^1S state. The doubly excited configurations I and III can couple to $1s\sigma_g^2 2p\sigma_u\lambda_u$ configurations, where λ_u is an orbital which yields an excited He of $n \geq 3$. These couplings could partially explain the optical excitation data, yet excitations of triplet states of He with cross sections comparable[48] to the higher (n = 3,4) singlet excitations seem to require a mechanism populating doubly excited asymptotes.[47]

Another secondary interaction that is possibly important even at low energies couples primary channel I with the $1s\sigma_g 2p\sigma_u^2 2s\sigma_g(^1\Sigma_g^+)$ state at their crossing near 1.5 a_o. This configuration has the excited He_2^+ core $1s\sigma_g 2p\sigma_u^2$ and like the $He_2^+(^2\Sigma_g^+)$ state is strongly repulsive at small internuclear distance. Asymptotically $1s\sigma_g\ 2p\sigma_u^2 2s\sigma_g$ would produce one 2s and three 1s electrons. Hence, it would seem to correlate to $He(1s^2)$ + $He(1s2s)2^1S$. However, the lower state $1s\sigma_g^2 2p\sigma_u 3p\sigma_u(^1\Sigma_g^+)$ with a $^2\Sigma_u^+$ He_2^+ core would also naively be associated with the same asymptote.

The difficulty lies in the extension of a molecular orbital picture to large distances. The incoming channel designated in the MO nomenclature $1s\sigma_g^2 2p\sigma_u^2$ can be unambiguously connected at large r with two ground state $He(1^1S)$ atoms. For

higher states, the MO configurations cannot be connected to a unique state of the separated atoms. For example, at very large distances, the configurations designated by $1s\sigma_g^2 2p\sigma_u 3p\sigma_u (^1\Sigma_g^+)$ and $1s\sigma_g 2p\sigma_u^2 2s\sigma_g (^1\Sigma_g^+)$ would be degenerate in a MO framework. Actually the two $^1\Sigma_g^+$ states can formally yield two different asymptotic atomic state pairs[33,50]

$$He(1s^2) + He(1s2s)^1S$$

and

$$He^+(1s) + He^-(1s^2 2s)^2S \quad .$$

Invoked here is a modification of the MO picture at large r, where it is difficult to apply, in favor of a description that connects in a reasonable way to the proper asymptotic states. A collision pair described by either of these $^1\Sigma_g^+$ configurations at small distance will evolve into the two asymptotic states in a way that depends on the couplings between them in the region where they interact.[50,52] At low velocities the higher $1s\sigma_g 2p\sigma_u^2 2s\sigma_g$ configuration will populate the $He^+ + He^-$ asymptote, and the $1s\sigma_g^2 2p\sigma_u 3p\sigma_u$ configuration will lead to the lower $He + He(2^1S)$ channel, assuming there are no important interactions with other states that are not considered in this simple picture. At higher velocities there will be a sharing of population between the two asymptotes.

Similar arguments can be made to connect the important $1s\sigma_g^2 2p\sigma_u 2p\pi_u (^1\Pi_g)$ configuration and the higher $1s\sigma_g 2p\sigma_u^2 3d\pi_g (^1\Pi_g)$ configuration with the asymptotic states $He(1s^2) + He(1s2p)^1P$ and $He^+(1s) + He^-(1s^2 2p)^2P$. The doubly excited $1s\sigma_g^2 2s\sigma_g^2$ configuration can be connected[50] with several $^1\Sigma_g^+$ ion pair states in addition to $He^*(1s2s) + He^*(1s2s)$.

The $He^-(1s^2 n\ell)$ states have never been observed, even as electron scattering resonances, but vanishing lifetimes at infinite separation do not preclude the possibility of their stabilization in the field of a nearby He^+ ion.[53] At large distances the $He^-(1s^2 2s) + He^+$ state lies[52] a couple of eV above the $He^+ + He + e$ continuum and autoionization processes would yield low energy electrons and a total loss of translational energy between the two nuclei of ~ 25 eV. For the excited core $1s\sigma_g 2p\sigma_u^2 2s\sigma_g$ configuration, molecular autoionization could also take place on the repulsive portion of the potential curve at small distances ($\lesssim 2.8\ a_o$) where the relevant potential is also above the lowest continuum.

The possibility of sharing of scattered intensity between two or more asymptotic states gives a convenient explanation for much of the ionization observed in He-He collisions. Gerber et al.[45,46] attribute an intense peak at an electron

energy of 19.3 eV to decay of the $He^{-*}(1s2s^2)\,^2S$ resonance, formed from $1s\sigma_g^{\,2}2p\sigma_u^{\,2} \rightleftharpoons 1s\sigma_g^{\,2}2s\sigma_g^{\,2} \rightarrow He^+ + He^-(1s2s^2)$. Other higher energy He^{-*} resonances which decay to $He^*(2^3S)$ or $He^*(1^1S)$ could be viewed as possible ionic dissociation paths from the channels responsible for the excitation of the higher optical states seen by Kempter et al.[48]

Both for single and double excitations, Brenot et al.[44] note strong similarities in the differential cross section shapes for excitation and ionization that imply possible sharing processes in the outgoing channels. They earlier suggested[43] that the double excitation III yielded $He^+ + He^-(1s2p^2)\,^2D$ as well as He(1s2p) + He(1s2p). The single excitation they attribute to primary excitation II followed by a sharing at large r between the $He(1s2p)\,^1P + He(1s^2)$ and the $He^-(1s^22p) + He^+(1s)$ asymptotes. Gauyacq[52] argues that the $He^-(1s^22p)$ decay gives a cross section significantly smaller than the data and is not as important as $He^-(1s^22s)$ for the ionization channel related to single excitation. He calculates the differential cross section for formation of $He^-(1s^22s)$ from the secondary processes

$$\text{II} \rightarrow 1s\sigma_g^{\,2}2p\sigma_u 3p\sigma_u \rightarrow \begin{cases} He^+ + He^-(1s^22s) \\ He + He(1s2s) \end{cases}$$

and

$$\text{I} \rightarrow 1s\sigma_g 2p\sigma_u^{\,2}2s\sigma_g \rightarrow \begin{cases} He^+ + He^-(1s^22s) \\ He + He(1s2s) \end{cases}$$

The result is a calculated cross section that is significantly larger than the one he calculates for $He^-(1s^22p)$ from the mechanism proposed by Barat et al.[43] Unfortunately, the shape of the calculated differential cross section does not satisfactorily agree with the data, and it is possible that $He^-(1s^22p)$ makes a larger relative contribution than indicated by the branching ratios in his calculations. A more complete treatment of the sharing between states that have the same limit in an MO picture should address possible interactions with other excited states of the same symmetry and should also account for possible autoionization at small or intermediate distances. It is difficult to evaluate the effect of these two additional complications on the calculated differential cross sections.

These same questions arise when considering He^* + He collisions. Even for this "simple" four electron system, there are enough complications to thwart a complete <u>ab initio</u> treatment for the inelastic scattering. Gauyacq's extensive <u>ab initio</u> calculations represent the most complete theoretical treatment of He-He scattering and have produced excellent agreement with much of the scattering data

including He^* + He interactions.[54] His work has helped introduce a useful framework for analyzing collisional ionization data; this framework can better be evaluated as more data become available.

Although He^* + He collisions explore many of the same potential surfaces as the ground state collision, there are significant important distinctions. The beam is a mixture of $He^*(2^1S)$ and $He^*(2^3S)$ and there are two potentials curves connecting to each He^* + He asymptote; this yields four incoming channels: $^1\Sigma_g^+$, $^1\Sigma_u^+$, $^3\Sigma_g^+$, and $^3\Sigma_u^+$, each of which must be considered in the analysis. Since the $He^*(2^3S)/He^*(2^1S)$ ratio in the beam is thought to be large, the data may mostly reflect contributions from the $He^*(2^3S)$ component. In the MO framework the $^1\Sigma_g^+$ state and the paired ($^1\Sigma_g^+$) $He^+ + He^-(1s^2 2s)\,^2S$ state are correlated to the $1s\sigma_g{}^2 2p\sigma_u 3p\sigma_u$ and $1s\sigma_g 2p\sigma_u{}^2 2s\sigma_g$ configurations as before, with analogous pairings for the other three symmetries. Hence in $^1\Sigma_g^+$ symmetry the incoming channels are identical to important product channels of He-He collisions and many of the theoretical calculations for He-He collisions can be utilized to extract information about He^* + He interactions.[54] Potential curves calculations[55,56] exist for states of other symmetry, but most dynamical calculations[33,54,57-59] treat either the $^1\Sigma_g^+$ or the $^3\Sigma_g^+$ incoming channels.

For a description of the experimental results, I will concentrate on the major inelastic channels observed; in all cases I will assume that the inelastic channels due to the ground state $He(1^1S)$ component of the metastable beam has been properly identified and removed.

At low c.m. energy (75-1100 eV) the total destruction cross section[17] has been measured separately for $He^*(2^1S)$ and $He^*(2^3S)$. Recently the $He^*(2^3S)$ result has been extended down to 11 eV using a different technique.[28] These are not true measurements of inelastic processes, for in each case a large fraction of the "destruction" cross section[60] will simply represent excitation transfer to the target atom. The true inelastic loss process

$$He^*(2^3S) + He \rightarrow He^*(2^3P) + He$$

will not even be detected (unless the excitation is transferred to the target) since a $He^*(2^3P)$ will quickly radiate back to $He^*(2^3S)$. For $He^*(2^1S)$ excitation to the 2^1P level, the radiation to 1^1S insures measurement of the attenuation; and it is interesting to observe that the measured total "destruction" cross section for $He^*(2^1S)$ is 3-6 $Å^2$ larger than for $He^*(2^3S)$ over the entire energy range[17] from 75-1100 eV.

Ab initio calculations of these 2s → 2p excitations give large cross sections at low energies. Rotational coupling of the $^3\Sigma_g^+$ incoming channel with the $^3\Pi_g$ state was predicted[8] to be the cause of significant perturbations observed in low energy $He^*(2^3S)$ + He elastic scattering data. The excitation cross section was estimated[58] to be 4 $Å^2$ at 100 eV and to be > 1 $Å^2$ at a collision energy of 9 eV, where the calculations were verified by tof measurements of the inelastic differential cross sections.[29] Radial coupling of the incoming $^3\Sigma_g^+$ curve to the $^3\Sigma_g^+$ curve which dissociates to $He^*(2^3P)$ + He is negligible at low energies, but is predicted to make a significant contribution to 2^3P excitation at energies above ~ 100 eV.[57] The analogous radial coupling mechanism for excitation of $He(2^1P)$ has not been calculated, but may be more important at low energies because the two relevant $^1\Sigma_g^+$ curves are closer in energy (at least asymptotically) than the $^3\Sigma_g^+$ curves. The $2^1S \rightarrow 2^1P$ transition associated with rotational coupling of the $^1\Sigma_g^+$ and $^1\Pi_g$ states has been calculated at low energies by Shipsey et al.[59] At 100 eV collision energy the excitation cross section is ~ 6 $Å^2$, which coincidentally agrees with the difference between measured $He^*(2^1S)$ and $He^*(2^3S)$ total destruction cross sections.[17] This suggests the importance of radiative cascade processes to the measured differences in destruction.

Detailed double differential cross section measurements[32] of the collisional ionization process exist in the c.m. energy range 50-200 eV. Fig. 3 shows a few typical energy loss spectra for $He^* + He \rightarrow He^+ + He + e^-$ for a beam energy of 197 eV. Four features are labelled A, B, C, and D and their properties and probable causes are summarized below.

Feature A is the major one at all measured scattering angles and is the dominant contribution to the total ionization cross section from threshold into the keV energy range. The c.m. energy loss ΔE of ~ 5 eV for feature A implies ground state He^+ + He products and a low energy emitted electron. The angular distribution peaks very sharply at 0^o and the threshold angle in a ρ vs. τ plot is much smaller than values found for ground state He-He inelastic processes. The ionization (for $He^*(2^1S)$) was explained by considering a diabatic $^1\Sigma_g^+$ potential as the primary incoming channel for the ionization process (see Fig. 4); at small distances this channel is strongly repulsive having character equivalent to the $1s\sigma_g 2p\sigma_u^2 2s\sigma_g$ MO configuration and matches the Frozen Orbital state calculated by Guberman and Goddard.[56] The diabatic state enters the continuum near the minimum of the $He_2^+(^2\Sigma_u^+)$ potential; and ionization is postulated to occur with significant probability at this crossing. Although no justification was

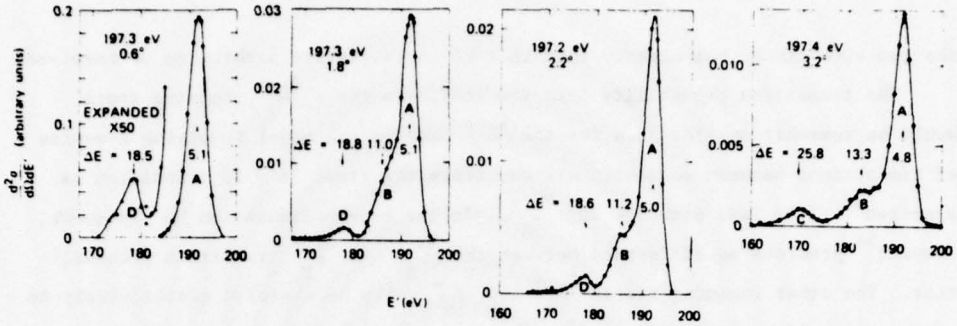

Fig. 3. He^+ product laboratory energy distributions for four scattering angles.

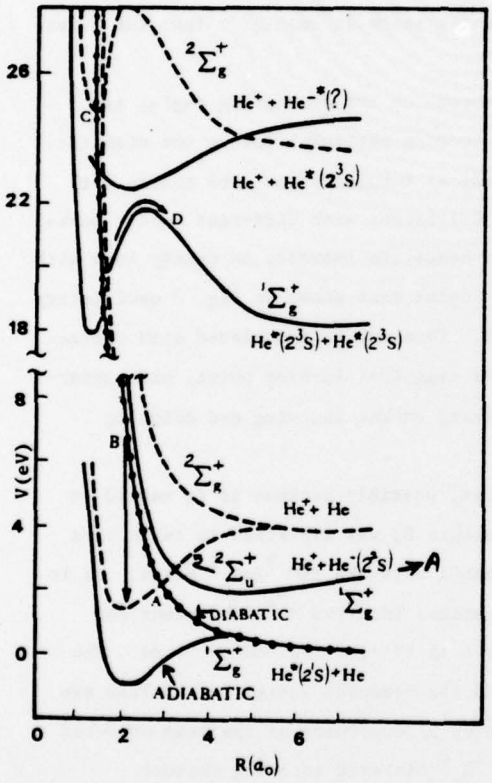

Fig. 4. A schematic representation of various potential curves of possible importance to collisional ionization. He_2^+ states are dashed; He_2 states solid.

given for that postulate, the calculated deflection functions indicated that the proposed mechanism adequately matched the most important features of the data. The probabilities of following the diabatic curve were related to the radial couplings between successively higher adiabatic $^1\Sigma_g^+$ curves starting with the $2^1S \rightarrow 2^1P$ radial coupling.[57] A transfer to the $He^+ + He^-(1s^2 2s)$ asymptote with ionization at large r was considered[32] as another possible mechanism consistent with feature A. This is in the spirit of Gauyacq's treatment of the He_2 system.[54] Yet that alternative treatment postulates (or at least assumes) no ionization at small r (which does exist as evidenced by other ionization features) and no interaction of the excited $He^+ + He^-(1s^2 2s)$ state with the series of Rydberg states of the same symmetry. The truth may lie somewhere between

the two viewpoints, but clearly this is a key interpretive problem to be resolved.

The transition probability into the continuum for a $^3\Sigma_g^+$ incoming state would be somewhat smaller than for the $^1\Sigma_g^+$ case in the model involving a series of transitions between adiabatic states, since the first 2s → 2p transition is expected[32] to be less probable for $^3\Sigma_g^+$. In the two-configuration MO framework, Gauyacq[54] predicts no difference between the $^1\Sigma_g^+$ and $^3\Sigma_g^+$ transition probabilities. The other incoming states $^1\Sigma_u^+$ and $^3\Sigma_u^+$ would be expected qualitatively to behave more adiabatically from either viewpoint and should contribute less to the important ionization channels; but there exists no quantitative evaluation of the differences.

The three other major ionization features can be explained by interactions involving the repulsive $1s\sigma_g 2p\sigma_u^2 2s\sigma_g$ diabatic state at smaller r than the crossing into the continuum at 2.8 a_o.

Process B, whose energy loss value depends on the scattering angle, is consistent with a mechanism in which the incoming particles follow the diabatic channel into the continuum, reach the classical turning point, and ionize with probability peaked at the turning point. Collisions with different impact parameter will reach different turning points; hence the increase in energy loss with scattering angle (see Fig. 4). At higher angles than shown in Fig. 3 oscillatory structure appears between features A and B. This may be associated with ionization between the continuum crossing and the classical turning point, with interference developing between collisions ionizing on the incoming and outgoing portions of the trajectory.[61]

Process D, visible only at small angles, possibly because it is masked at the larger angles by contributions from feature B, was explained in terms of a coupling of the $1s\sigma_g 2p\sigma_u^2 2s\sigma_g$ incoming channel with the $1s\sigma_g^2 2s\sigma_g^2$ state. As in He-He scattering, the $1s\sigma_g^2 2s\sigma_g^2$ state separates into two $He^*(2^3S)$ atoms and molecular autoionization at large r yields a 15 eV electron and He^+ + He. The shape of the differential cross section and the measured energy loss values are consistent with a suggestion[33] that the $He^*(2^1S)$ component of the beam produces this feature by interactions following the $^1\Sigma_g^+$ diabatic incoming channel. Gauyacq's calculations[54] indicate that this process has a very small cross section; and he hypothesizes that the $He^*(2^3S)$ component of the beam may analogously contribute to this feature through a coupling of $^3\Sigma_u^+$ potentials.

Features A, B and D all involve scattering at small angles, since in each case there are significant attractive interactions along the outgoing trajectory

to at least partially compensate for the initial repulsive encounter along the diabatic potential. Feature C has threshold and angular dependence more typical of inelastic transitions in other systems. The energy loss of 25-27 eV suggests formation of an excited product atom and low energy electrons

$$He^* + He \rightarrow He^+ + He^* + e \quad ,$$

and the angular threshold is consistent with ionization occurring at the crossing into the first excited continuum (see Fig. 4). However, contributions from transitions $1s\sigma_g 2p\sigma_u {}^2 2s\sigma_g \rightarrow 1s\sigma_g {}^2 2s\sigma_g n\sigma$, which could produce $He^+ + He^-(1s2sn\ell)$, cannot be excluded.

At larger scattering angles and higher collision energies, more violent encounters at smaller r should yield rotational coupling processes in the united atom limit that are analogous to those observed in He-He collisions. The recent work of Morgenstern et al.[30] at collision energies from 500 to 2500 eV clearly shows effects due to coupling of the $2p\sigma_u$ and $2p\pi_u$ orbitals at small r. Nonetheless, the ionization channels mentioned above, especially feature A, are still probably the most important ionization channels at these higher energies. The electron energy distribution, which peaks very strongly at an energy near 0 eV and drops monotonically at higher energies, agrees qualitatively with the distribution anticipated to be associated with the major low energy ionization features; yet an unknown fraction of these electrons could be produced by electron ejection from surfaces following an excitation transfer of metastable energy to a slow target He atom. This experimental problem is peculiar to electron energy measurements in collisions of metastable beams with large internal energy, and precludes a definitive conclusion based on the electron energy distributions.

The only discrete structure observed in the electron spectra[30] are a set of peaks near 35 eV due to autoionization of doubly excited He^{**} and a couple of peaks at 19.3 and 19.7 eV thought associated with production of $He^-(1s2s^2)$ and $He^-(1s2s2p)\,{}^4P$ states respectively. The energies of the peaks from He^{**} indicate that the $2s2p({}^3P)$ and $2p^2({}^1D)$ states give the major contributions. Generally, for each peak in the electron energy distribution at the proper energy, there is a companion peak at a shifted energy. This companion peak is due to decays of excited projectiles, whose electrons are Doppler shifted in energy relative to those produced by decay of the same state of the excited target atom.[62] Interestingly, the peak at 19.7 eV has no companion peak and the result is consistent with the authors' observation[30] that the long ($\gtrsim$ 10 μsec) lifetime of the ${}^4P$ He^- state

allows excited projectile ions to leave the observation zone before emitting an electron. Similarly a fraction of the slow He^- target may escape detection.

The inelastic scattering results[30] using tof techniques indicate a strong $\sim$ 20 eV excitation, a smaller $\sim$ 60 eV excitation, and an even smaller $\sim$ 40 eV excitation. The resolution was not sufficient to identify any states, but clearly inelastic channels yielding two excited atoms are quite important and it is also evident that the He^{**} autoionizing states are more often formed paired with an excited He^* partner ($\Delta E = 60$) than with a ground state He($\Delta E = 40$) .

The primary inelastic channel can be explained by rotational coupling between a $2p\sigma_u$ and $2p\pi_u$ orbital, for example,

$$1s\sigma_g 2p\sigma_u{}^2 2s\sigma_g (^{1,3}\Sigma_g^+) \rightarrow 1s\sigma_g 2p\sigma_u 2p\pi_u 2s\sigma_g \rightarrow He^*(1s2s) + He^*(1s2p) \quad ,$$

or

$$1s\sigma_g{}^2 2p\sigma_u 2s\sigma_g (^{1,3}\Sigma_u^+) \rightarrow 1s\sigma_g{}^2 2p\pi_u 2s\sigma_g \rightarrow He^*(1s2s) + He^*(1s2p) \quad .$$

This excitation can also produce the $He^-(1s2s2p)\ ^4P$ observed in electron energy measurements. The potential coupling mechanism

$$1s\sigma_g 2p\sigma_u{}^2 2s\sigma_g (^1\Sigma_g^+) \rightarrow 1s\sigma_g{}^2 2s\sigma_g{}^2 (^1\Sigma_g^+)$$

can likewise yield two excited atoms, but the absence of 15 eV electrons corresponding to the long range molecular autoionization process[33] observed at lower energies suggests that this process may not be very important at these energies.

Two step rotational coupling in the united atom limit, e.g.

$$1s\sigma_g 2p\sigma_u{}^2 2s\sigma_g \rightarrow 1s\sigma_g 2p\pi_u{}^2 2s\sigma_g \quad ,$$

is probably the main mechanism responsible for the 60 eV excitation and the production of the observed $He(2s2p)\ ^3P$ and $He(2p^2)\ ^1D$ autoionizing levels.

Morgenstern et al.[30] point out that the mechanisms they have examined all involve no active participation by the 2s electron. Like the $1s\sigma_g$ electron, it is a spectator to the collision until the outgoing channel when it must choose a nucleus to follow. Their measurements were not, of course, sensitive to other excitation and ionization channels (e.g., $2s \rightarrow n\ell$ excitations or process B described at lower energies) where the 2s electron participates actively in the inelastic process.

ACKNOWLEDGEMENTS

I thank R. Morgenstern and J. P. Gauyacq for communicating results prior to publication. Discussions with D. L. Huestis and R. E. Olson are appreciated.

References

*Supported in part by the Office of Naval Research and the National Science Foundation

1. R. M. Hill, D. L. Huestis, and C. K. Rhodes in Laser Induced Fusion and X-ray Laser Studies, Vol. 3, eds. Stephen F. Jacobs, et al. (Addison Wesley, 1976) p. 277; D. C. Lorents, X ICPEAC, Paris 1977, Invited Lecture.
2. See, for example, D. W. Martin, T. Fukuyama, R. W. Gregor, R. M. Jordan, and P. E. Siska, J. Chem. Phys. 65, 3720 (1976) and references cited therein.
3. B. Brutschy and H. Haberland, Phys. Rev. Letters 38, 686 (1977).
4. S. M. Trujillo, IX ICPEAC Seattle 1975, Abstracts of Papers, 437, 439, 953.
5. See, for example, reviews by V. Sidis IX ICPEAC Seattle 1975, Invited Lectures, Review Papers and Progress Reports, 295; V. Kempter, ibid., 327; R. Morgenstern, ibid., 345; M. Barat, VIII ICPEAC Beograd 1973, Invited Lectures and Progress Reports, 43; and R. McCarroll, ibid., 71.
6. H. Haberland, X ICPEAC Paris 1977, Progress Report.
7. J. R. Peterson and D. C. Lorents, Phys. Rev. 182, 152 (1969).
8. R. Morgenstern, D. C. Lorents, J. R. Peterson, and R. E. Olson, Phys. Rev. A 8, 2372 (1973).
9. See also R. J. Girnius and L. W. Anderson, Nucl. Inst. and Methods 137, 373 (1976); and references therein.
10. R. E. Olson and F. T. Smith, Phys. Rev. A 7, 1529 (1973); E. L. Duman, VII ICPEAC Amsterdam 1971, Abstracts of Papers, 471.
11a. R. E. Olson, E. J. Shipsey, and J. C. Browne (unpublished).
11b. C. F. Melius, Sandia Laboratories (unpublished).
12. G. E. Ice and R. E. Olson, Phys. Rev. A 11, 111 (1975).
13. A. Salop, D. C. Lorents, and J. R. Peterson, J. Chem. Phys. 54, 1187 (1971).
14. G. Lantschner, Thesis, "Ionizationsprozesse beim Stoss von schnellem metastabilem Helium mit Edelgasatomen," Freiburg University (1975).
15. R. H. Neynaber and G. D. Magnuson, J. Chem. Phys. 65, 5239 (1976).
16. K. T. Gillen, R. P. Saxon, D. C. Lorents, G. E. Ice, and R. E. Olson, J. Chem. Phys. 64, 1925 (1976).
17. M. Hollstein, J. R. Sheridan, J. R. Peterson, and D. C. Lorents, Phys. Rev. 187, 118 (1969).
18a. H. Hotop, A. Niehaus, and A. L. Schmeltekopf, Z. Phys. 229, 1 (1969).
18b. F. B. Dunning, T. B. Cook, W. P. West, and R. F. Stebbings, Rev. Sci. Inst. 46, 1072 (1975).
19. C. N. Burrous, A. J. Lieber, and V. T. Zaviantseff, Rev. Sci. Instr. 38, 1477 (1967).
20. J. K. Layton, J. Chem. Phys. 59, 5744 (1973).
21. R. Morgenstern, M. Barat, and D. C. Lorents, J. Phys. B 6, L330 (1973).
22. K. T. Gillen, R. P. Saxon, and D. C. Lorents, Phys. Rev. A 13, 2033 (1976).
23. G. Spiess, K. T. Gillen, and R. P. Saxon, J. Phys. B 10, 899 (1977).
24. G. D. Magnuson and R. H. Neynaber, J. Chem. Phys. 60, 3385 (1974); R. H. Neynaber and G. D. Magnuson, J. Chem. Phys. 62, 4953 (1975).
25. M. Hollstein, A. Salop, J. R. Peterson, and D. C. Lorents, Phys. Letters 32A, 327 (1970).
26. R. H. Neynaber, G. D. Magnuson, and J. K. Layton, J. Chem. Phys. 57, 5128 (1972).
27. A. P. Kalinin and V. B. Leonas, Sov. Phys. Dokl. 18, 323 (1973) [Dokl. Acad. Nauk SSSR 210, 316 (1973)].
28. T. M. Miller, X ICPEAC Paris, 1977, Abstracts, 466.

29. R. E. Olson, R. Morgenstern, D. C. Lorents, J. C. Browne, and L. Lenamon, Phys. Rev. A 8, 2387 (1973).
30. R. Morgenstern, E. Schade, and M. Trainer, J. Phys. B. (in press); see also X ICPEAC, Paris, 1977, Abstracts, 458.
31. K. T. Gillen, D. C. Lorents, R. E. Olson, and J. R. Peterson, J. Phys. B 7, L327 (1974).
32. K. T. Gillen, J. R. Peterson, and R. E. Olson, Phys. Rev. A 15, 527 (1977).
33. R. P. Saxon, K. T. Gillen, and B. Liu, Phys. Rev. A 15, 543 (1977).
34. R. H. Neynaber and G. D. Magnuson, Phys. Rev. A 12, 891 (1975).
35. J. T. Moseley, J. R. Peterson, D. C. Lorents, and M. Hollstein, Phys. Rev. A 6, 1025 (1972).
36. M. L. Coleman, R. Hammond, and J. Dubrin, Chem. Phys. Letters 19, 271 (1973).
37. A. P. Kalinin and V. B. Leonas, JETP Letters 21, 339 (1975) [Zh ETP Pis. Red. 21, 715 (1975)].
38. G. Lantschner and A. Niehaus, Chem. Phys. Letters 23, 223 (1973).
39. C. Rebick and J. Dubrin, J. Chem. Phys. 55, 5825 (1971).
40. R. H. Neynaber and G. D. Magnuson, Phys. Rev. A 11, 865 (1975).
41. R. H. Neynaber and G. D. Magnuson, Phys. Rev. A 14, 961 (1976).
42. See, for example, J. A. Aten, G. E. H. Lanting, and J. Los, Chem. Phys. 19, 241 (1977); and references cited therein.
43. M. Barat, D. Dhuicq, R. Francois, C. Lesech, and R. McCarroll, J. Phys. B 6, 1206 (1973).
44. J. C. Brenot, D. Dhuicq, J. P. Gauyacq, J. Pommier, V. Sidis, M. Barat, and E. Pollack, Phys. Rev. A 11, 1245 (1975).
45. G. Gerber, R. Morgenstern, and A. Niehaus, J. Phys. B 6, 493 (1973).
46. G. Gerber and A. Niehaus, J. Phys. B 9, 123 (1976).
47. V. Kempter, F. Veith, and L. Zehnle, J. Phys. B 8, 1041 (1975).
48. V. Kempter, G. Riecke, F. Veith and L. Zehnle, J. Phys. B 9, 3081 (1976).
49. W. Lichten, Phys. Rev. 164, 131 (1967); M. Barat and W. Lichten, Phys. Rev. A 6, 211 (1972).
50. J. P. Gauyacq, J. Phys. B 9, 2289 (1976).
51. R. E. Olson, E. J. Shipsey, and J. C. Browne, J. Phys. B 8, 905 (1975).
52. J. P. Gauyacq, J. Phys. B 9, 3067 (1976).
53. See also H. S. Taylor, F. W. Bobrowicz, P. J. Hay, and T. H. Dunning, Jr., J. Chem. Phys. 65, 1182 (1976); H. S. Taylor, E. Goldstein, and G. A. Segal, X ICPEAC 1977, Abstracts, 796.
54. J. P. Gauyacq, Thesis, Orsay (1977), unpublished.
55. See, for example, M. L. Ginter and R. Battino, J. Chem. Phys. 52, 4469 (1970); W. J. Steets and N. F. Lane, Phys. Rev. A 11, 1994 (1975); and J. S. Cohen, Phys. Rev. A 13, 86 (1976).
56. S. L. Guberman and W. A. Goddard III, Phys. Rev. A 12, 1203 (1975).
57. S. A. Evans, J. S. Cohen, and N. F. Lane, Phys. Rev. A 4, 2235 (1971).
58. L. Lenamon, J. C. Browne, and R. E. Olson, Phys. Rev. A 8, 2380 (1973).
59. E. J. Shipsey, J. C. Browne, and R. E. Olson, Phys. Rev. A 11, 1334 (1975).
60. S. A. Evans and N. F. Lane, Phys. Rev. 188, 268 (1969).
61. V. Sidis, J. Phys. B 6, 1188 (1973).
62. For a discussion, see Ref. 45.
63. J. Pommier, Vu Ngoc Tuan, and M. Barat, X ICPEAC Paris, 1977, Abstracts, 456.
64. S.F.W. Harper and A.C.H. Smith, X ICPEAC Paris, 1977, Abstracts, 82.
65. Several experiments first reported in the ICPEAC, Paris, 1977, Abstracts Book could not be included in Table I, but should be mentioned. See. G. H. Bearman, H. H. Harris, and J. J. Leventhal, p. 286; R. H. Neynaber and G. D. Magnuson, p. 312; and M. Durup and G. Pavlant, p. 468.

Appendix D

$He(2^3S)$ DEEXCITATION IN COLLISIONS WITH $He(1^1S)$

$He(2^3S)$ DEEXCITATION IN COLLISIONS WITH $He(1^1S)$*

THOMAS M. MILLER

Molecular Physics Center, Stanford Research Institute
Menlo Park, CA 94025

The deexcitation of metastable $He(2^3S)$ atoms in collisions with ground-state helium has been studied using a beam-gas technique over a center-of-mass (CM) energy range of 11-86 eV. Essentially all of the deexcitation is due to excitation transfer from projectile atoms to target gas atoms:[1]

$$He(2^3S) + He(1^1S) \rightarrow He(1^1S) + He(2^3S)$$

This experiment is an extension to low energies of the work in this laboratory by Hollstein, Sheridan, Peterson, and Lorents,[1] who covered the CM energy range 75-1100 eV.

One motivation for the present work is provided by the calculations of Evans and Lane[2] whose excitation-transfer cross sections for $He(2^3S)$ are shown in Fig. 1. Also shown are the present data and the low-energy data of Hollstein et al.[1] It is hoped that calculations with better He_2 potentials which are now available will improve the comparison between experiment and theory.

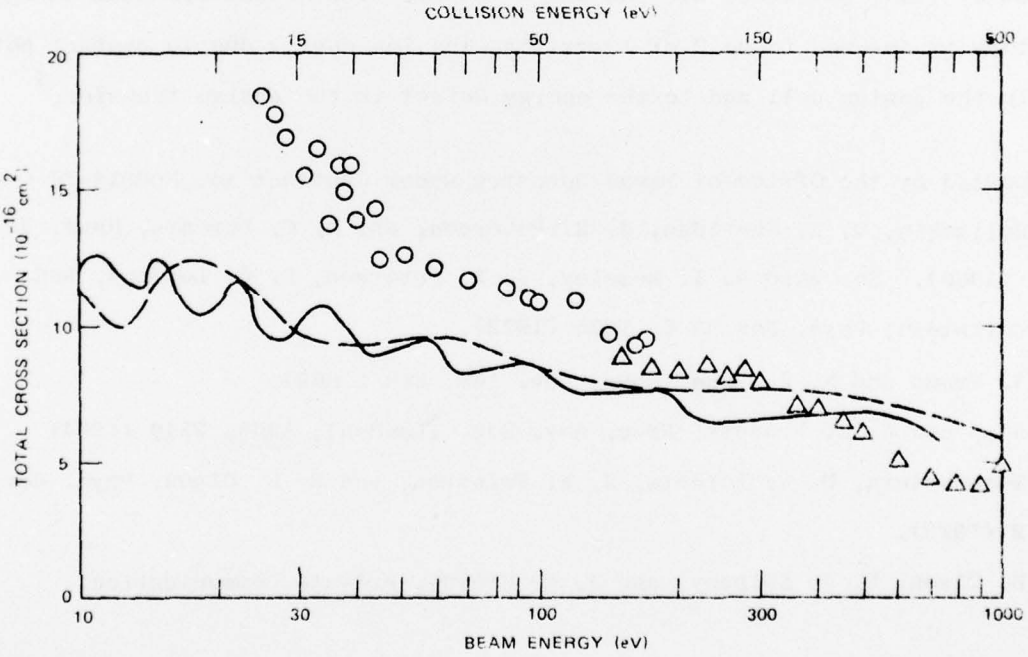

Fig. 1. $He(2^3S)$ excitation transfer cross section. Solid curve: Evans and Lane, diabatic. Dashed curve: Evans and Lane, adiabatic. Triangles: Data of Hollstein et al. Circles: present data.

As a consistency check on the low-energy data, we measured charge-transfer cross sections for $He^+ + He \rightarrow He + He^+$ and found agreement with previous data and the Rapp and Francis[3] results.

In the experiment of Hollstein et al.[1] an optical technique was used to determine the attenuation of the metastable beam in a helium gas cell. Their technique allowed definite identification of singlet and triplet events. In the present experiment the results are attributed to $He(2^3S)$ on the basis of experimental evidence[4] and recent calculations.[5] The metastable beam is produced by charge transfer in a cesium vapor cell. Attenuation of the metastable beam in a helium gas cell is determined from measurements of the beam intensity using a particle multiplier. Both the target gas pressure and the interaction path length are varied in order to minimize uncertainties. A correction is applied to the data to account for the partial detection of ground-state atoms in the beam. The correction is based on data obtained by Morgenstern et al.[4] in this laboratory, and amounts to 3% at 25 eV (CM), 30% at 61 eV, and 50% at 80 eV. The metastable atom energy in the laboratory is assumed to be 2 eV lower than the ion energy due to contact potentials in the cesium cell and to the energy defect in the charge transfer.[4]

* Supported by the Office of Naval Research under Contract No. N00014-76-C-0118.

1 M. Hollstein, J. R. Sheridan, J. R. Peterson, and D. C. Lorents, Phys. Rev. 187, 118 (1969). See also J. T. Moseley, J. R. Peterson, D. C. Lorents, and M. Hollstein, Phys. Rev. A 6, 1025 (1972).

2 S. A. Evans and N. F. Lane, Phys. Rev. 188, 268 (1969).

3 D. Rapp and W. E. Francis, Proc. Roy. Soc. (London), A268, 2349 (1964).

4 R. Morgenstern, D. C. Lorents, J. R. Peterson, and R. E. Olson, Phys. Rev. A 8, 2372 (1973).

5 R. E. Olson, E. J. Shipsey, and J. C. Browne, private communication.